

AD-A102 481 TERRA TEK INC SALT LAKE CITY UT
SIMULATION OF THE LOAD-UNLOAD PATHS EXPERIENCED BY ROCK IN THE --ETC(U)
DEC 77 D R SCHMITZ, J N JOHNSON, R K DROPEK DNA001-76-C-0294
UNCLASSIFIED TR-76-74 DNA-4841F NL

1 OF 1
AD-A
1024H

END
DATA
8-81
DTIC

ADA102481

DTIC FILE COPY

LEVEL ~~10~~ DNA 4841F

SIMULATION OF THE LOAD-UNLOAD PATHS EXPERIENCED BY ROCK IN THE VICINITY OF BURIED EXPLOSIONS

J. N. Johnson

R. K. Drokek

D. R. Schmitz

Terra Tek, Incorporated

420 Wakara Way

Salt Lake City, Utah 84108



1 December 1977

Final Report for Period 1 May 1976-1 December 1977

CONTRACT No. DNA 001-76-C-0294

APPROVED FOR PUBLIC RELEASE;
DISTRIBUTION UNLIMITED.

THIS WORK SPONSORED BY THE DEFENSE NUCLEAR AGENCY
UNDER RDT&E RMSS CODE B344076464 Y99QAXSB04903 H2590D.

Prepared for
Director
DEFENSE NUCLEAR AGENCY
Washington, D. C. 20305

81 8 05 008

Destroy this report when it is no longer
needed. Do not return to sender.

PLEASE NOTIFY THE DEFENSE NUCLEAR AGENCY,
ATTN: STTI, WASHINGTON, D.C. 20305, IF
YOUR ADDRESS IS INCORRECT, IF YOU WISH TO
BE DELETED FROM THE DISTRIBUTION LIST, OR
IF THE ADDRESSEE IS NO LONGER EMPLOYED BY
YOUR ORGANIZATION.



UNCLASSIFIED

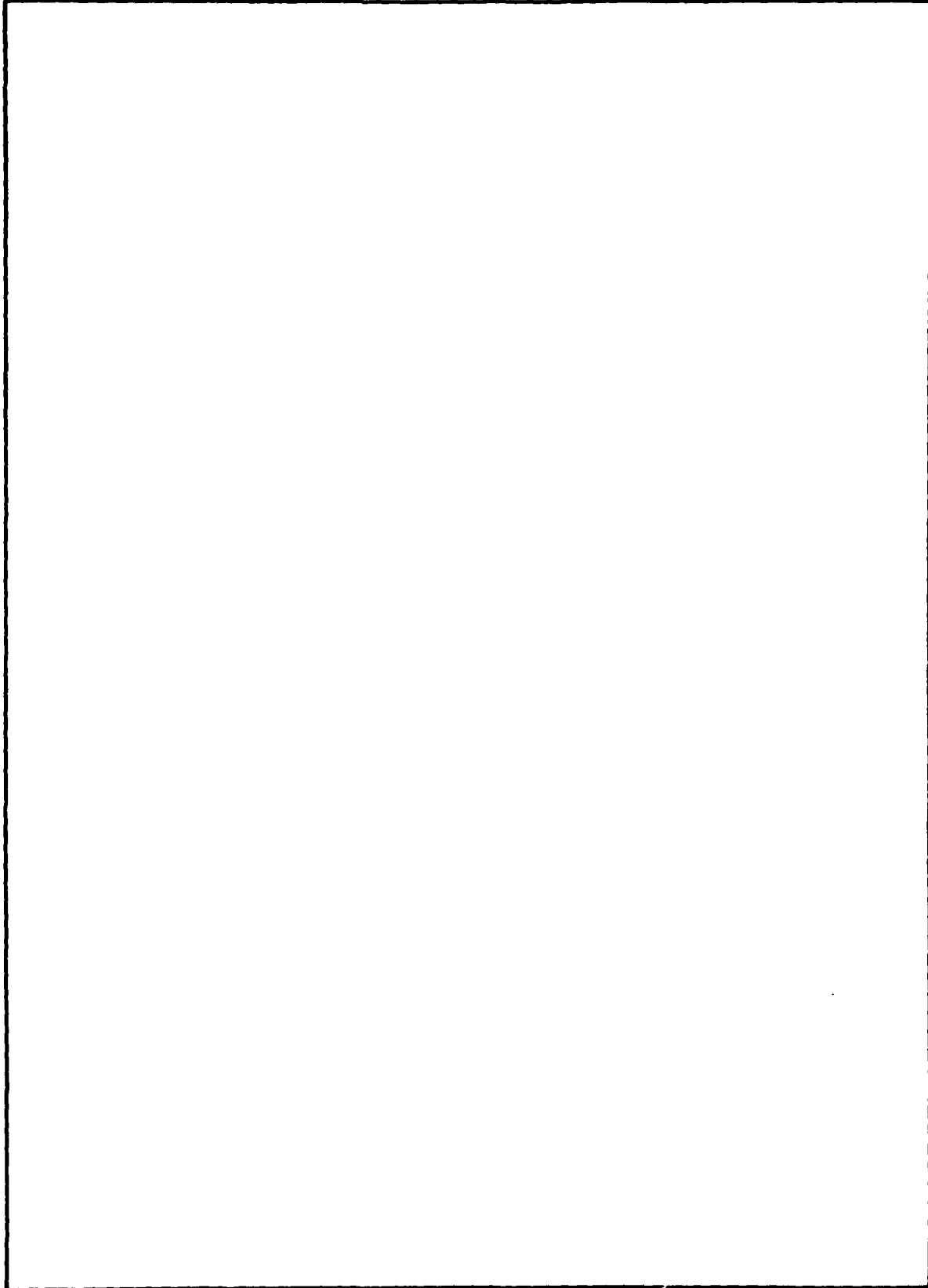
SECURITY CLASSIFICATION OF THIS PAGE (When Data Entered)

19. REPORT DOCUMENTATION PAGE		READ INSTRUCTIONS BEFORE COMPLETING FORM
1. REPORT NUMBER DNA 4841F	2. GOVT ACCESSION NO. AD-A102 482	3. RECIPIENT'S CATALOG NUMBER
4. TITLE (and Subtitle) SIMULATION OF THE LOAD-UNLOAD PATHS EXPERIENCED BY ROCK IN THE VICINITY OF BURIED EXPLOSIONS	5. TYPE OF REPORT & PERIOD COVERED 9 Final Report for Period 1 May 76 - 1 Dec 77	
6. PERFORMING ORG. REPORT NUMBER TR-76-74	7. AUTHOR(s) D. R. Schmitz J. N. Johnson R. K. Droeck	
8. CONTRACT OR GRANT NUMBER(s) DNA 001-76-C-0294	9. PERFORMING ORGANIZATION NAME AND ADDRESS Terra Tek, Inc. 420 Wakara Way Salt Lake City, UT 84108	
10. PROGRAM ELEMENT, PROJECT, TASK AREA & WORK UNIT NUMBERS Subtask Y99QAXSB049-03	11. CONTROLLING OFFICE NAME AND ADDRESS Director Defense Nuclear Agency Washington, D.C. 20305	
12. REPORT DATE 1 December 1977	13. NUMBER OF PAGES 62	
14. MONITORING AGENCY NAME & ADDRESS (if different from Controlling Office)	15. SECURITY CLASS. (of this report) UNCLASSIFIED	
16. DECLASSIFICATION/DOWNGRADING SCHEDULE N/A	17. DISTRIBUTION STATEMENT (of this Report) Approved for public release; distribution unlimited	
18. DISTRIBUTION STATEMENT (of the abstract entered in Block 20, if different from Report)		
19. SUPPLEMENTARY NOTES This work sponsored by the Defense Nuclear Agency under RDT&E RMSS Code B344076464 Y99QAXSB04903 H2590D.		
20. KEY WORDS (Continue on reverse side if necessary and identify by block number) Kayenta Sandstone Strain and Stress Paths Buried Explosions Finite Difference Solutions		
21. ABSTRACT (Continue on reverse side if necessary and identify by block number) Theoretical and experimental results are presented which define the strain paths and stress paths experienced by geological material elements in the vicinity of buried explosions. The theoretical strain and stress paths are obtained by finite-difference solution of spherical and cylindrical explosions in an infinite inelastic medium. These calculations are used to define loading and unloading paths in static laboratory tests on Kayenta sandstone. The data presented here thus provide the necessary information for definition of material constitutive models which apply to these specific explosive geometries.		

389435 x.1

UNCLASSIFIED

SECURITY CLASSIFICATION OF THIS PAGE(When Data Entered)



UNCLASSIFIED

SECURITY CLASSIFICATION OF THIS PAGE(When Data Entered)

TABLE OF CONTENTS

	<u>Page</u>
List of Illustrations.	1
List of Tables	4
Introduction	5
Stress Path Determination from Finite-Difference Solutions	6
Calculational Results	7
Static Experimental Simulation of Load-Unload Paths.	20
Test Results	23
Discussion and Conclusions	35
Appendix I	37
General Relationships and Finite-Difference Calculations.	37
Analytical Determination of Elastic Stress and Strain Paths for a Spherical Explosion	42
Appendix II.	47
Specimen Preparation.	47
Stress and Strain Determination	47
Testing Procedures.	48
Data Acquisition and Analysis	48

LIST OF ILLUSTRATIONS

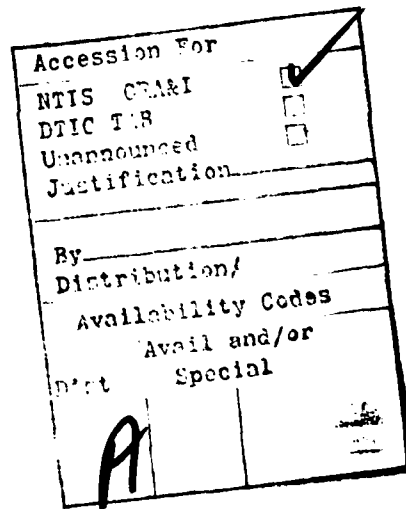
<u>Figure Number</u>		<u>Page</u>
1a	Strain paths and stress paths at $R = 2R_0$ cylindrical wave propagation in Mixed Company sandstone	9
1b	Same as 1a, but with $R = 3R_0$	10
1c	Same as 1a, but with $R = 5R_0$	11
2a	Strain paths and stress paths at $R = 1.5R_0$ for spherical wave propagation in Mixed Company sandstone	12

LIST OF ILLUSTRATIONS (Cont)

<u>Figure Number</u>		<u>Page</u>
2b	Same as 2a, but with $R = 2R_0$. Note changes in vertical and horizontal scales	13
2c	Same as 2a, but with $R = 3R_0$. Note changes in vertical and horizontal scales	14
2d	Same as 2a, but with $R = 4R_0$. Note changes in vertical and horizontal scales	15
2e	Same as 2a, but with $R = 5R_0$. Note changes in vertical and horizontal scales	16
3	Strain paths and stress paths at various positions for cylindrical wave propagation in Mixed Company sandstone	17
4a	Comparison of the theoretical (calculated) strain path to the experimental strain path to be followed during testing of path I ($1/\alpha = 0.1$ msec)	21
4b	Comparison of the theoretical (calculated) strain path to the experimental strain path to be followed during testing of path II ($1/\alpha = 1.0$ msec)	21
4c	Comparison of the theoretical (calculated) strain path to the experimental strain path to be followed during testing of path III ($1/\alpha = 10$ msec)	22
5a	Strain path followed during uniaxial-strain loading and constant-axial and uniaxial-strain unloading	24
5b	Stress path followed during uniaxial-strain loading and constant-axial and uniaxial-strain unloading	24
6a	Strain path followed during uniaxial-strain loading and constant-axial-strain unloading	25
6b	Stress path followed during uniaxial-strain loading and constant-axial-strain unloading	25
7a	Strain path followed during uniaxial-strain loading and constant-volume-strain unloading	26
7b	Stress path followed during uniaxial-strain-loading and constant-volume-strain unloading	26
8	Comparison of strain and stress paths determined numerically and analytically for spherical wave propagation in an elastic medium	46
9	Pressure vessel schematic showing the sample and stress and strain transducers	49

LIST OF ILLUSTRATIONS (Cont)

<u>Figure Number</u>		<u>Page</u>
9a	Stress path followed during strain path III testing . . .	50
9b	Strain path followed during path I testing	51
9c	Stress path followed during strain path II testing . . .	52
9d	Strain path followed during path II testing	53
9e	Stress path followed during strain path I testing	54
9f	Strain path followed during path III testing	55



LIST OF TABLES

<u>Table Number</u>	<u>Description</u>	<u>Page</u>
Ia	1236 Test Results	27
Ib	1239 Test Results	28
IIa	1241 Test Results	29
IIb	1257 Test Results	30
IIc	1285 Test Results	31
IIIa	1269 Test Results	32
IIIb	1270 Test Results	33
IIIc	1284 Test Results	34

INTRODUCTION

Common testing procedures for the laboratory measurement of material properties for use in ground motion calculations have generally consisted of standard hydrostatic, uniaxial-strain and triaxial tests. It has recently been recognized that these paths are not necessarily the ones that are followed in actual field applications, i.e., conventional and nuclear explosions in the earth. Since difficulty is often experienced in developing accurate constitutive models that are valid for a wide range of loading conditions, it seems important to follow, as closely as possible, the stress paths (or strain paths) that are experienced by material elements in actual field conditions. Furthermore, since measurement techniques do not yet allow the field determination of these stress paths (or strain paths), one must rely on numerical calculations and an initial best estimation of the material constitutive properties. In this report we present the results of one-dimensional numerical finite-difference calculations for cylindrical and spherical wave propagation, which define the stress and strain paths followed by material elements at varying distances from cylindrical and spherical explosive sources in the earth. The purpose of these calculations is to define laboratory tests best suited for the definition of material constitutive behavior in the analysis of CIST (Cylindrical In Situ Tests) and other subsurface explosive events. On the basis of these calculational results, static laboratory tests are conducted which represent strain paths experienced by material elements in the vicinity of cylindrical and spherical explosions in an infinite medium. The material tested in the experimental program is Kayenta sandstone.

STRESS PATH DETERMINATION FROM FINITE-DIFFERENCE SOLUTIONS

The quantities which are obtained from the finite-difference solution are σ_i and ϵ_i as functions of time at various distances from the explosive source. For purposes of definite laboratory tests, it is useful to express the output of these calculations in terms of the load $L = \sigma_a - p_c$ and p_c in the triaxial test configuration. Here σ_a is the axial stress and p_c is the confining fluid pressure. It is also more convenient to deal with axial and transverse strain components (ϵ_a and ϵ_t) in the triaxial test rather than ϵ_i defined in the finite-difference solution. In the case of spherical flow, one would simply make the identification that $L = \sigma_1 - \sigma_3$, $p_c = \sigma_3$, $\epsilon_a = \epsilon_1$, and $\epsilon_t = \epsilon_3$. For cylindrical flow the identification is slightly more complicated.

In general, let us assume that we have values of stress and strain invariants defined by

$$\tau(t) = [(\sigma_1 - \sigma_2)^2 + (\sigma_2 - \sigma_3)^2 + (\sigma_3 - \sigma_1)^2]^{1/2} / \sqrt{6} \quad , \quad (1)$$

$$p(t) = (\sigma_1 + \sigma_2 + \sigma_3) / 3 \quad , \quad (2)$$

$$\epsilon_v(t) = \epsilon_1 + \epsilon_2 + \epsilon_3 \quad , \quad (3)$$

$$\epsilon_d(t) = [(\epsilon_1 - \epsilon_2)^2 + (\epsilon_2 - \epsilon_3)^2 + (\epsilon_3 - \epsilon_1)^2]^{1/2} / \sqrt{6} \quad , \quad (4)$$

as functions of time at a fixed spatial position as provided by the finite-difference calculation. If the material constitutive behavior involves only first and second invariants of the stress and strain tensors, the quantities defined by Eqs. (1) - (4) can also be written in the following terms for the purpose of defining laboratory test paths:

$$\tau(t) = (\sigma_a - p_c)/\sqrt{3} , \quad (5)$$

$$p(t) = (\sigma_a + 2p_c)/3 , \quad (6)$$

$$\epsilon_v(t) = \epsilon_a + 2\epsilon_t , \quad (7)$$

$$\epsilon_d(t) = (\epsilon_a - \epsilon_t)/\sqrt{3} , \quad (8)$$

and hence laboratory stress and strain paths become in parametric form (t as the parameter):

$$L = \sqrt{3} \tau(t) , \quad (9)$$

$$p_c = p(t) - \tau(t)/\sqrt{3} , \quad (10)$$

$$\epsilon_a = \epsilon_v(t)/3 + 2\epsilon_d(t)/\sqrt{3} , \quad (11)$$

$$\epsilon_t = \epsilon_v(t)/3 - \epsilon_d(t)/\sqrt{3} . \quad (12)$$

Calculational Results

Stress (and strain) paths for cylindrical and spherical wave propagation have been calculated with the use of elastic-plastic constitutive descriptions presented in the Appendix. The material parameters are chosen to be representative of Mixed Company (Kayenta) sandstone. In all cases a radial stress given by

$$\sigma_r = p_0 e^{-\alpha t} \quad (13)$$

is applied at the interior cavity surface of radius $R_0 = 1$ m. The peak radial stress, p_0 , is taken to be 10 kbar and the decay constant, $1/\alpha$, takes on values of 0.1 msec, 1.0 msec and 10 msec. All results are presented in

terms of ϵ_a vs. ϵ_t (axial strain vs. transverse strain) and L/μ vs. p_c/K (load/shear-modulus vs. confining-fluid-pressure/bulk-modulus), i.e., the quantities related directly to static triaxial laboratory tests.

Figures 1a, 1b and 1c show stress and strain paths at various distances from a cylindrical explosion. At the radial position $R = 2R_0$ the stress path intersects the failure surface during loading and remains in contact during unloading. The corresponding strain path initially approximates conditions of uniaxial strain, but exhibits considerable transverse strain during the latter stages of deformation. At $R = 3R_0$ it can be seen that the strain path is approximated by loading in uniaxial strain followed by unloading at constant axial strain, while at $R = 5R_0$ the axial strain is seen to decrease during unloading. Of course, at much greater distances from the explosive source plane-wave conditions are achieved, and the load-unload path remains on the $\epsilon_t = 0$ axis.

Figures 2a - 2e show similar behavior for spherical wave propagation. Figures 1 and 2 give an indication of how strain and stress paths depend on distance from the source. Another important consideration is that of pulse shape or pulse duration. This is controlled by the parameter α in Eq. (13). A number of calculations were performed for cylindrical geometry with $1/\alpha = 0.1$ msec, 1.0 msec and 10 msec. The peak radial stress p_0 remains the same in all calculations ($p_0 = 10$ kbar). The resulting stress and strain paths are shown in Figure 3 at radial positions $1.5R_0$, $2R_0$, $3R_0$, $4R_0$ and $5R_0$. One sees immediately that not only does the position have influence on stress and strain paths, but also that pulse duration has a significant effect. It will therefore be important to represent, as accurately as possible, the time history of the cavity stress due to the explosive source.

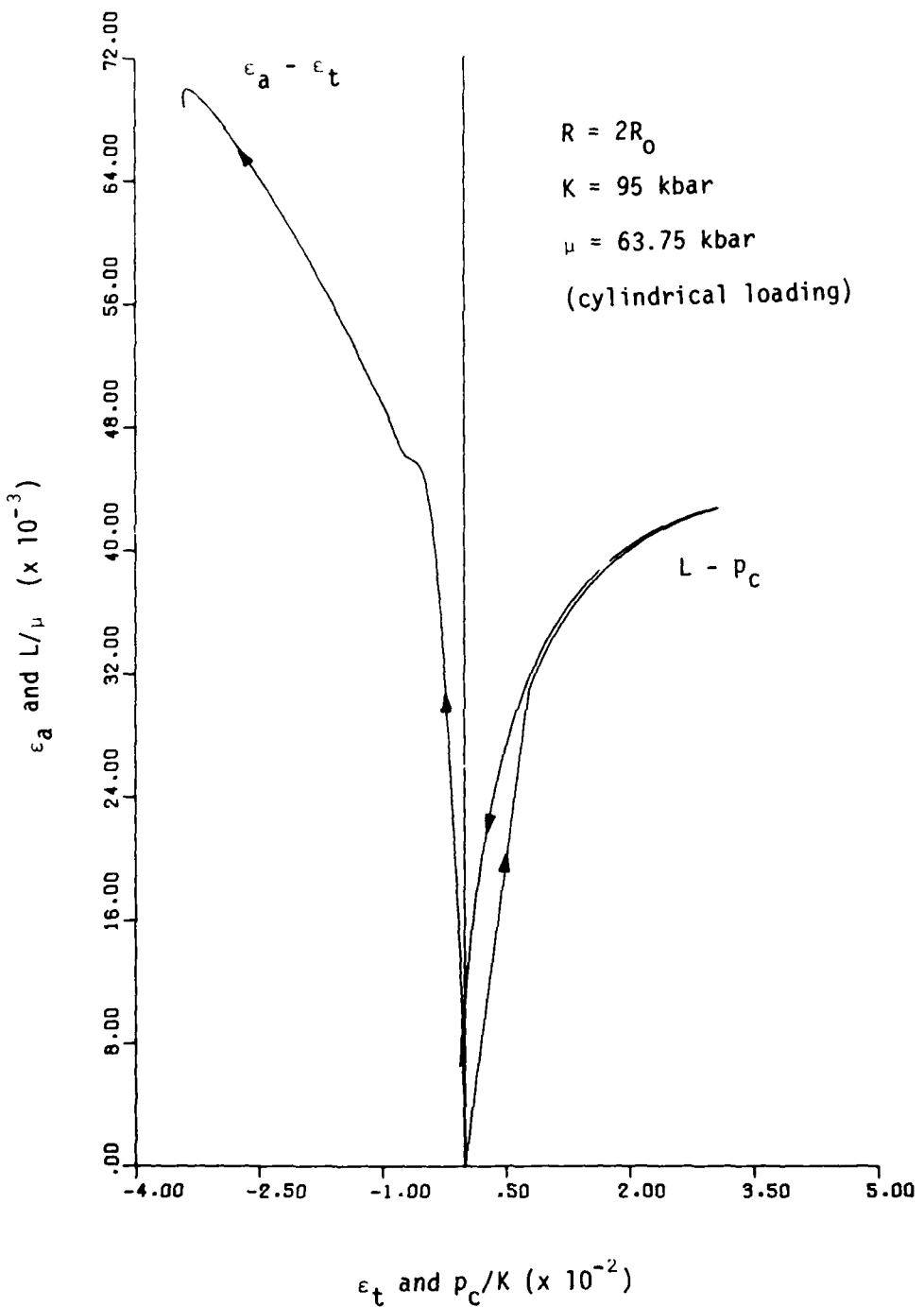


Figure 1a. Strain paths and stress paths at $R = 2R_0$ cylindrical wave propagation in Mixed Company sandstone. A radial stress given by $\sigma_r = p_0 \exp(-\alpha t)$, with $(1/\alpha) \approx 1 \text{ msec}$ and $p_0 = 10 \text{ kbar}$, is applied at $R_0 = 1 \text{ m}$.

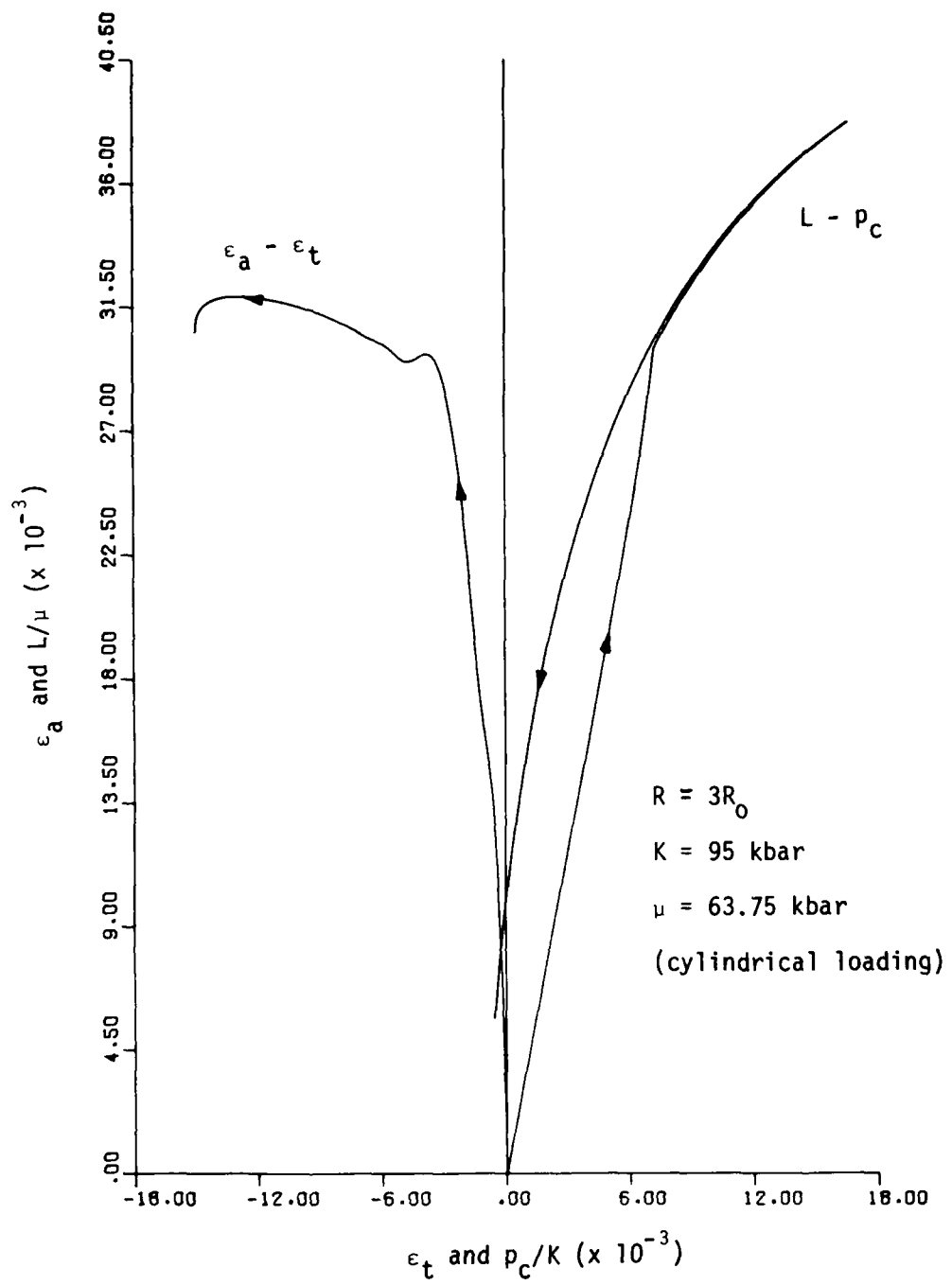


Figure 1b. Same as 1a, but with $R = 3R_0$. Note changes in vertical and horizontal scales.

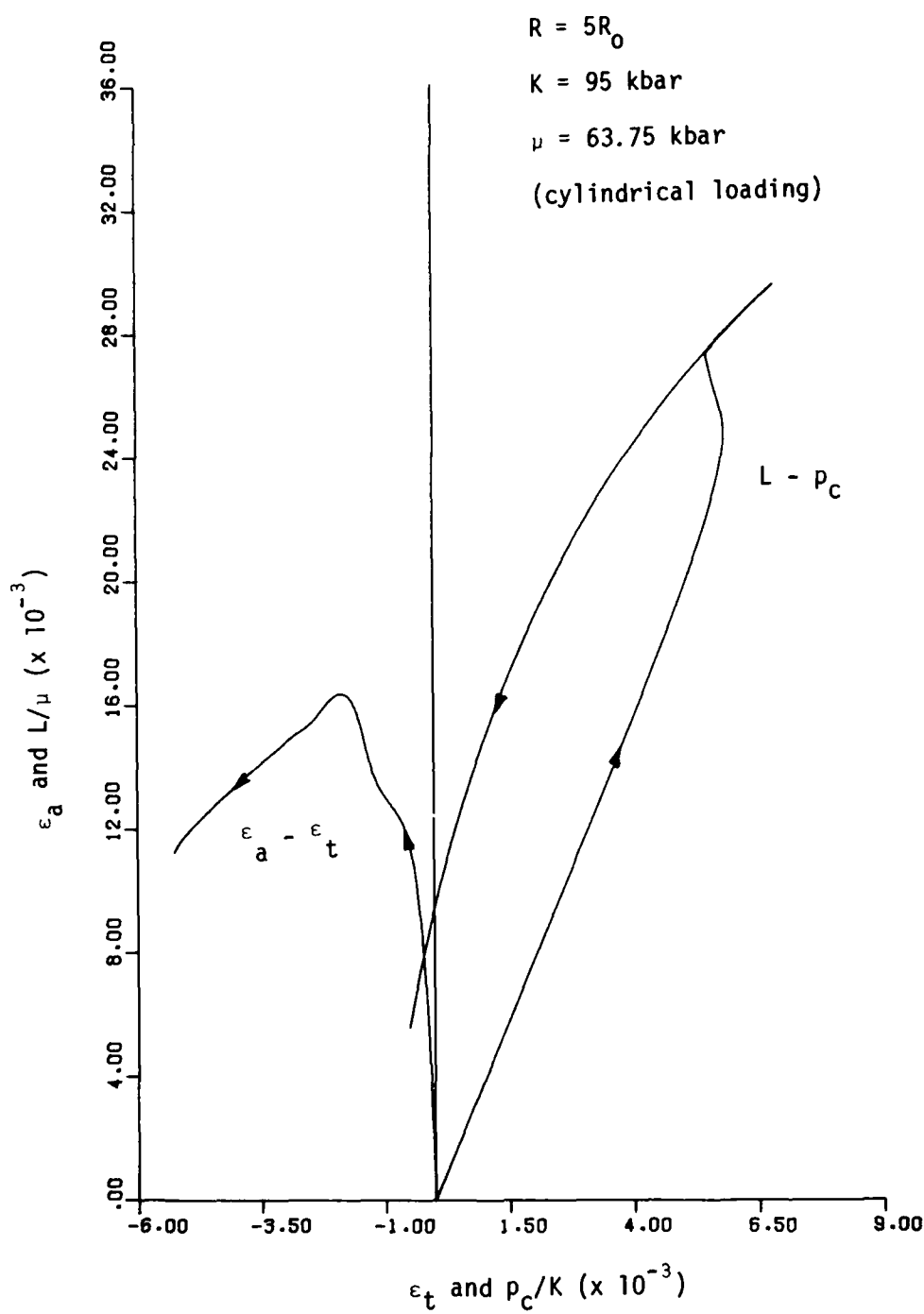


Figure 1c. Same as 1a, but with $R = 5R_0$. Note changes in vertical and horizontal scales.

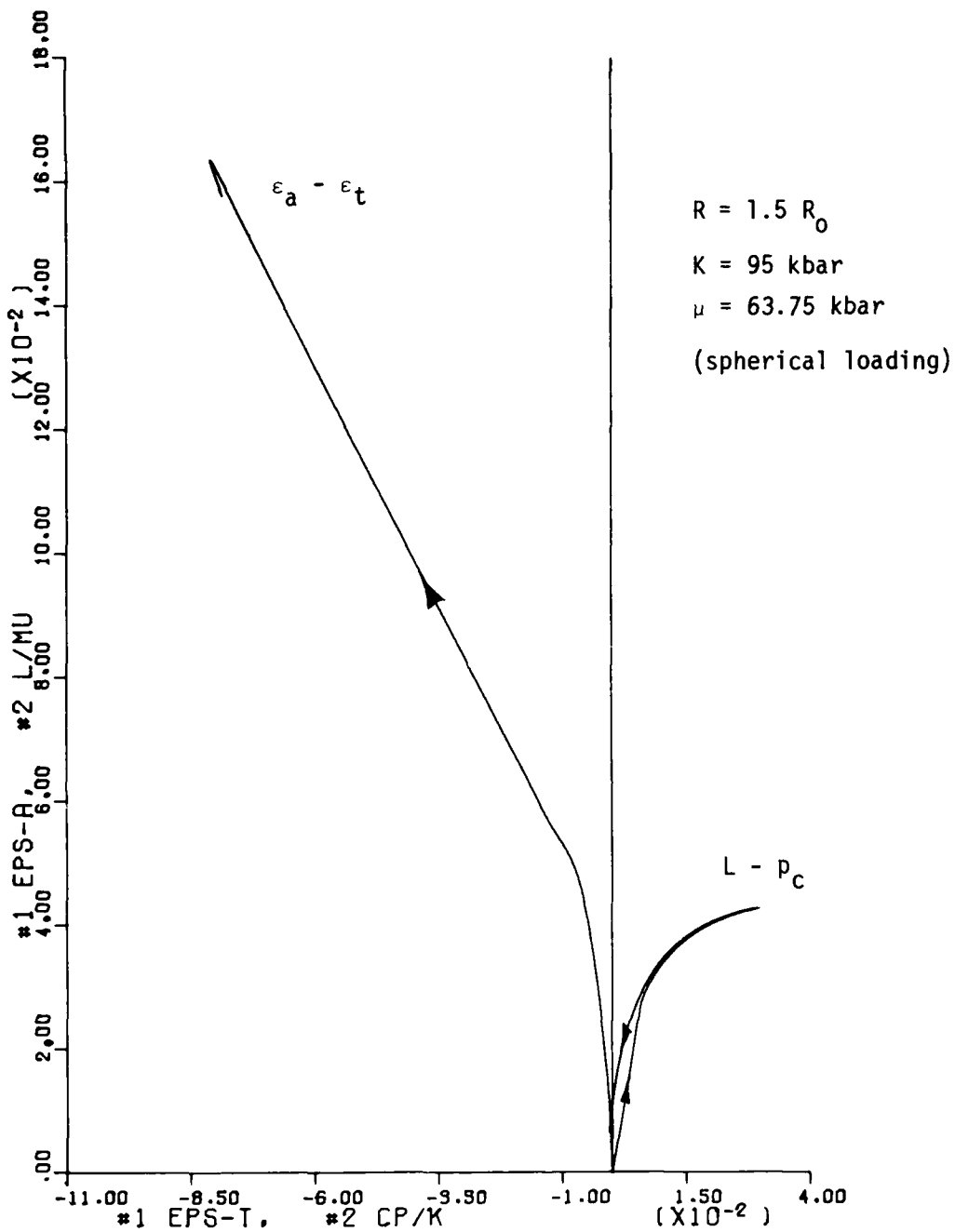


Figure 2a. Strain paths and stress paths at $R = 1.5R_0$ for spherical wave propagation in Mixed Company sandstone. A radial stress given by $\sigma_r = p_0 \exp(-\alpha t)$, with $1/\alpha = 1$ msec and $p_0 = 10$ kbar, is applied at $R_0 = 1$ m.

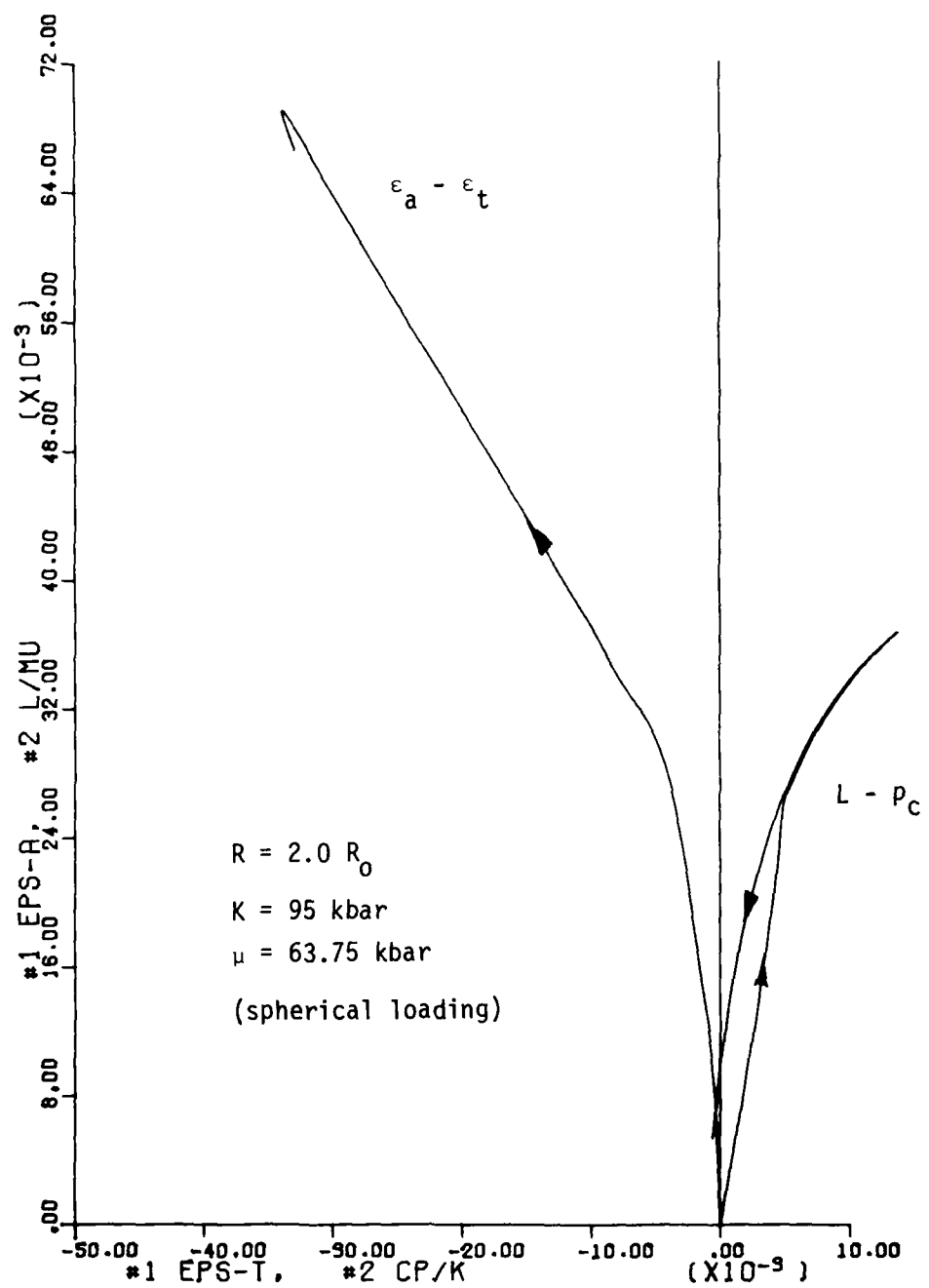


Figure 2b. Same as 2a, but with $R = 2R_0$. Note changes in vertical and horizontal scales.

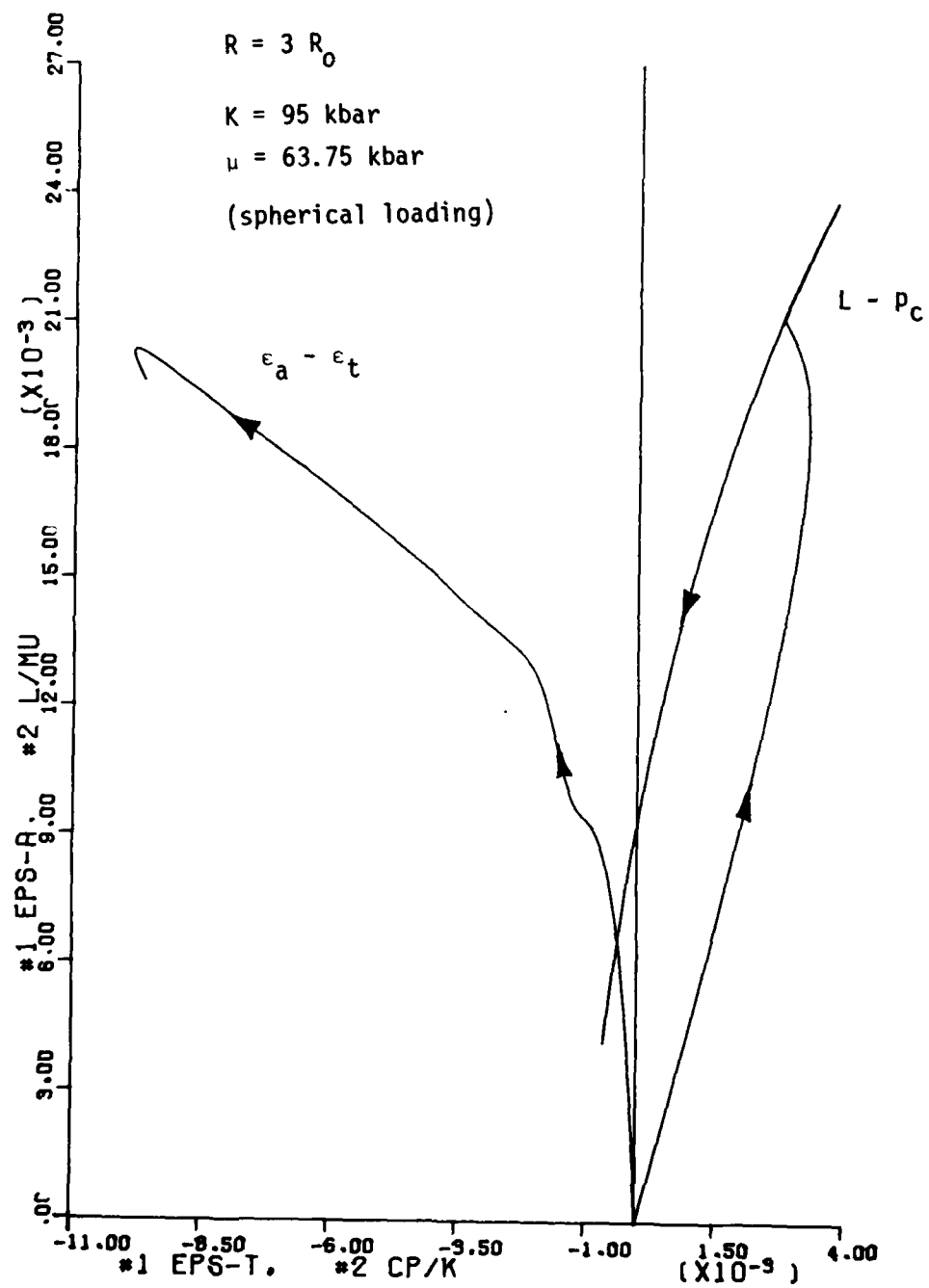


Figure 2c. Same as 2a, but with $R = 3R_0$. Note changes in vertical and horizontal scales.

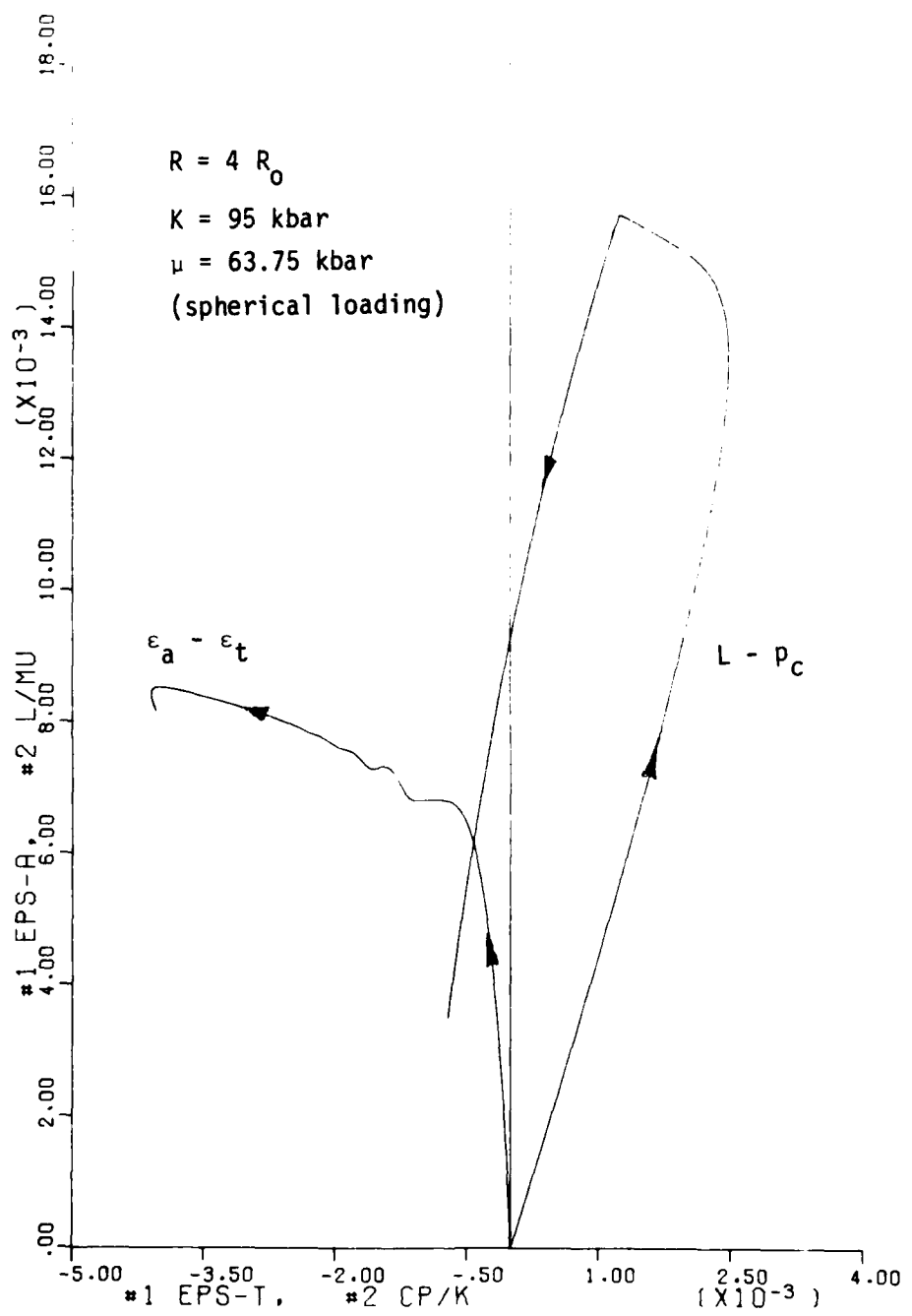


Figure 2d. Same as 2a, but with $R = 4R_0$. Note changes in vertical and horizontal scales.

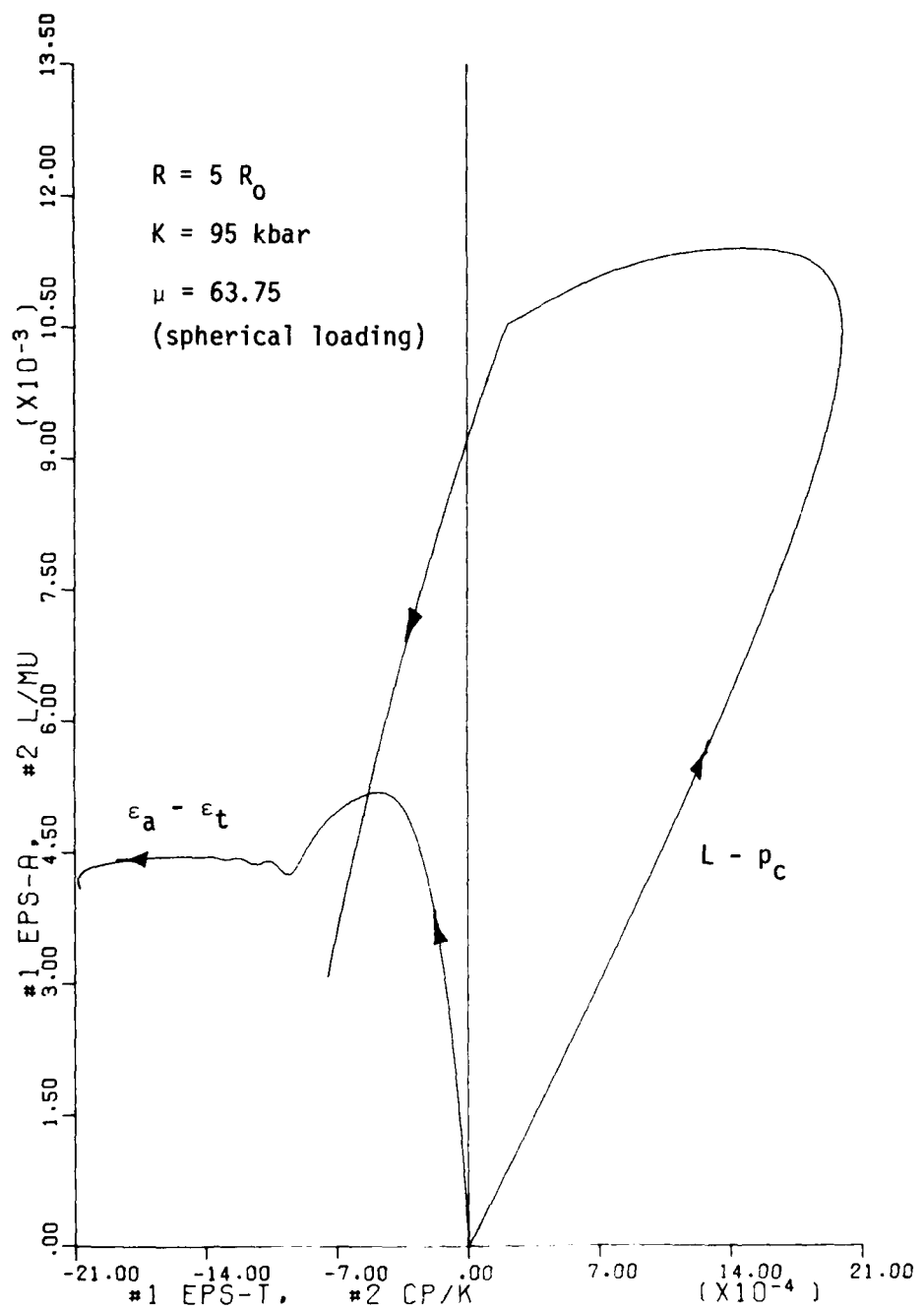


Figure 2e. Same as 2a, but with $R = 5R_0$. Note changes in vertical and horizontal scales.

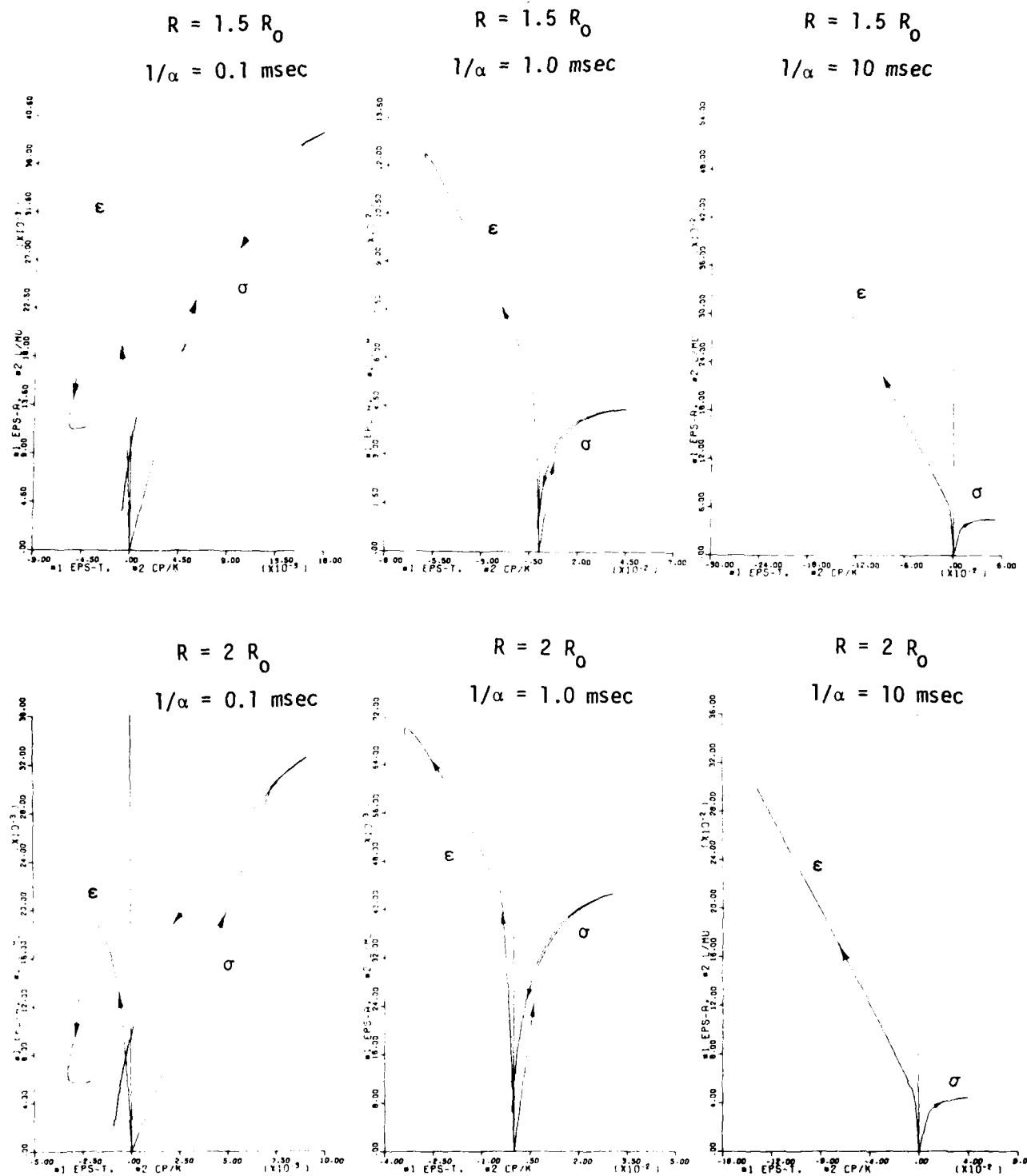


Figure 3. Strain paths and stress paths at various positions for cylindrical wave propagation in Mixed Company sandstone. A radial stress given by $\sigma_r = p_0 \exp(-\alpha t)$, with $p_0 = 10$ kbar and various values of $1/\alpha$, is applied at $R = 1\text{m}$. Note changes in the vertical and horizontal scales in each graph.

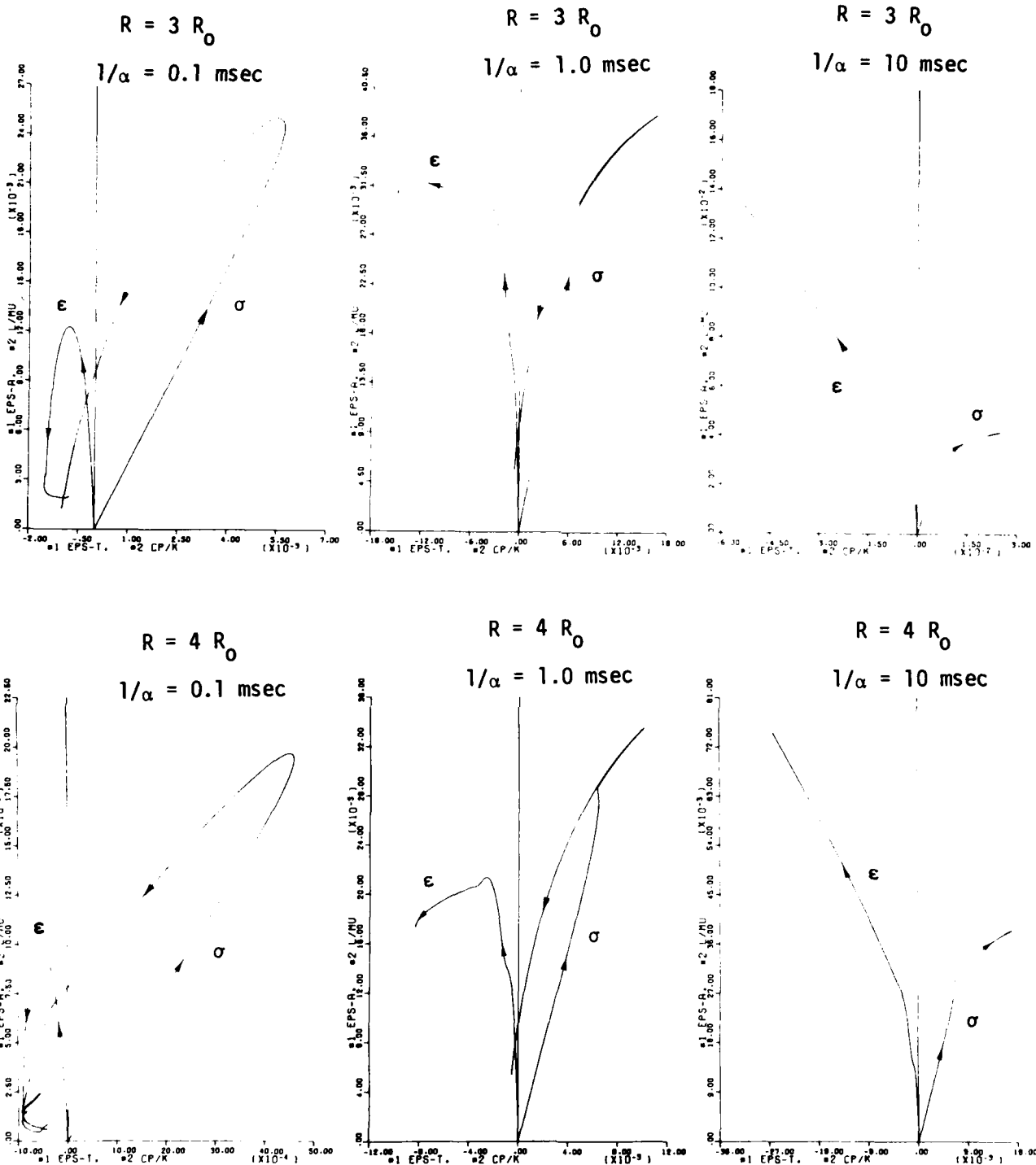


Figure 3. Continued.

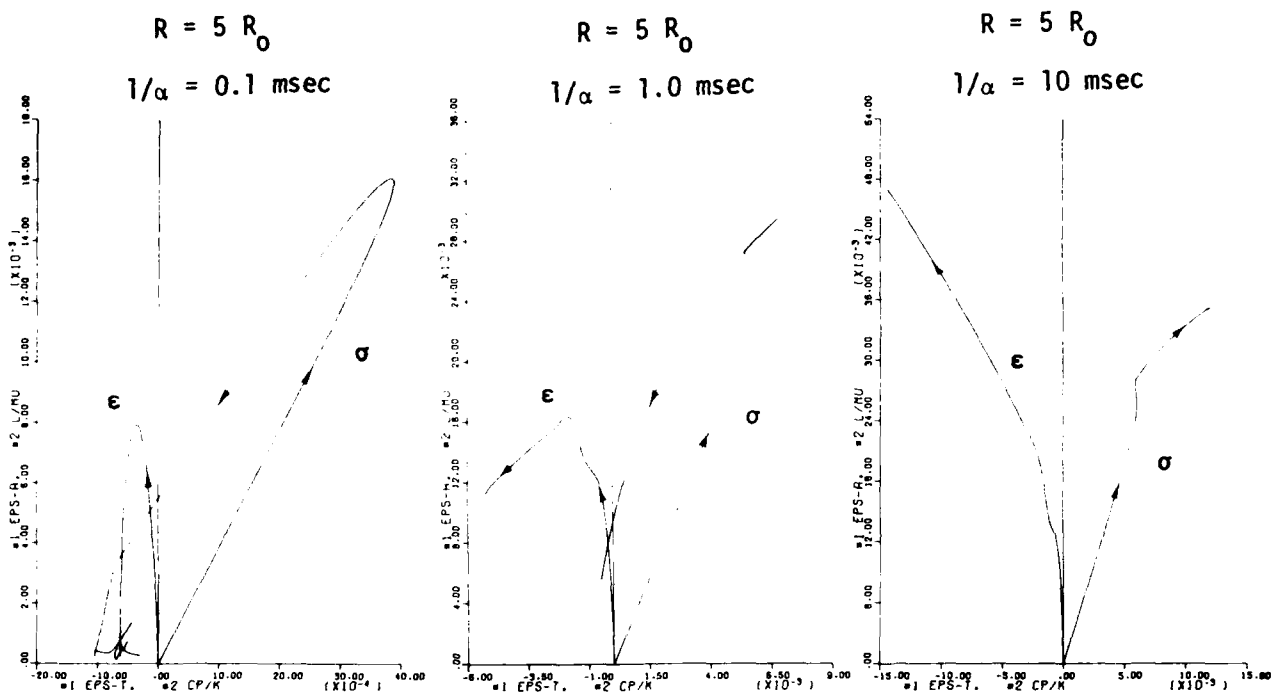


Figure 3. Continued.

STATIC EXPERIMENTAL SIMULATION OF LOAD-UNLOAD PATHS

Stress and strain paths were determined experimentally in the (L, p_c) and (ϵ_a, ϵ_t) planes using the results suggested by various one-dimensional finite-difference solutions given previously. A detailed discussion of experimental techniques used in these tests is presented in Appendix II. The stress and strain paths considered here correspond approximately to those given in Figure 3 for $R = 3R_0$ and three separate decay constants ($1/\alpha = 0.1$ msec, 1.0 msec and 10 msec). Figures 4a, 4b and 4c show the three characteristic strain paths generated from the numerical solution and the strain paths to be followed in the static laboratory tests. The percent strains indicated here are used only to indicate orders of magnitude and are not the actual values achieved during testing. No attempt was made to follow the numerically determined strain paths exactly; they were used simply to indicate the *qualitative* nature of load-unload paths in the vicinity of buried explosions. Figure 4a shows the calculated and experimental paths corresponding to a decay time of $1/\alpha = 0.1$ msec; this consists essentially of uniaxial-strain loading and constant-axial-strain unloading followed by uniaxial-strain unloading. Figure 4b shows the theoretical path corresponding to $1/\alpha = 10$ msec in comparison to the experimentally followed path. The experimental strain path to be used consists of a uniaxial-strain loading and a constant-axial-strain unloading. Finally Figure 4c shows the theoretical path for $1/\alpha = 10$ msec in comparison to the experimentally followed path. The experimental strain path to be used consists of uniaxial-strain loading and constant-volume-strain unloading. Kayenta sandstone from the Mixed Company site was the material tested in this investigation.

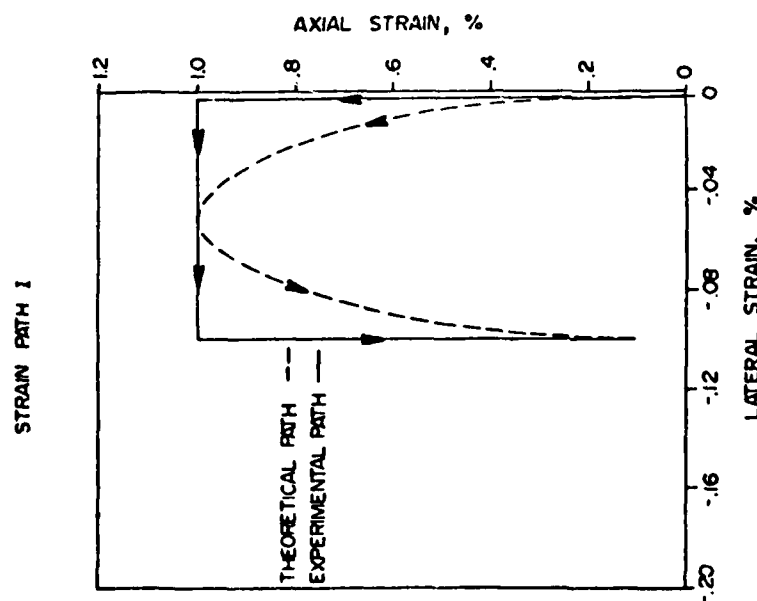


Figure 4a. Comparison of the theoretical (calculated) strain path to the experimental strain path to be followed during testing of path I ($1/\alpha = 0.1$ msec). The experimental path shows a uniaxial-strain loading followed by a constant-axial and uniaxial-strain unloading. The percent strains indicated here are used only to indicate orders of magnitude and are not the actual values achieved during testing.

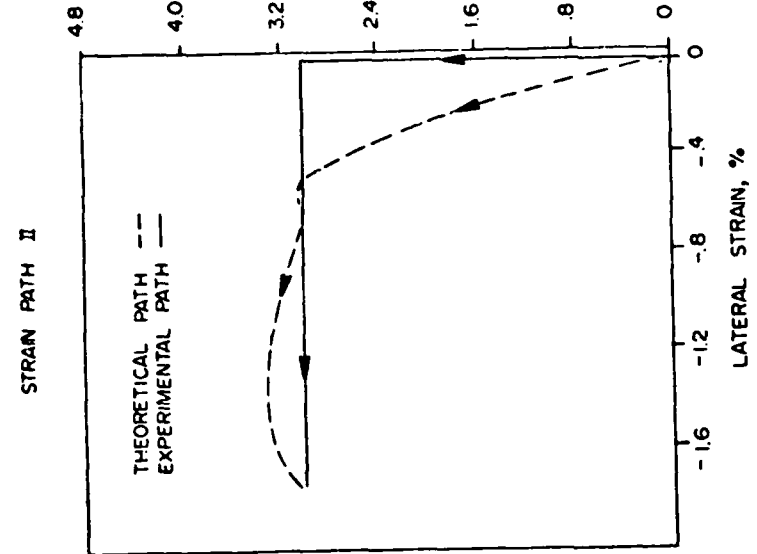


Figure 4b. Comparison of the theoretical (calculated) strain path to the experimental strain path to be followed during testing of path II ($1/\alpha = 1.0$ msec). The experimental path shows a uniaxial-strain loading followed by a constant-axial-strain unloading. The percent strains indicated here are used to indicate orders of magnitude and are not the actual values achieved during testing.

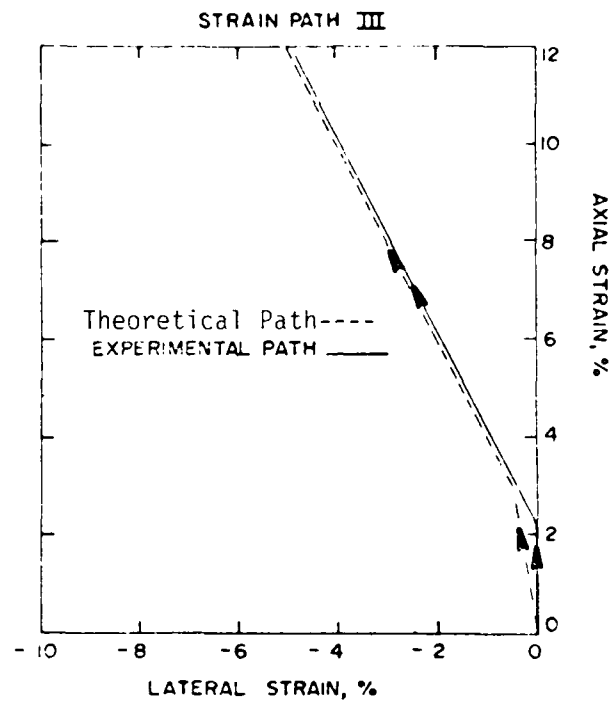


Figure 4c. Comparison of the theoretical (calculated) strain path to the experimental strain path to be followed during testing of path III ($1/\alpha = 10$ msec). The experimental path shows a uniaxial-strain loading with a constant-volume-strain unloading. The percent strains indicated here are used only to indicate orders of magnitude and are not the actual values achieved during testing.

TEST RESULTS

The three strain paths, I, II and III, used in testing the Kayenta sandstone are shown in Figures 5a, 6a and 7a, respectively. Since all loading was conducted under uniaxial-strain conditions, a composite loading curve is shown for each path type. Individual unloading curves are shown for each test, departing from the composite loading curve at their respective maximum strains. The stress paths generated from the three strain paths are shown in Figures 5b, 6b and 7b. Composite loading curves are shown along with individual unloading curves. Included in each stress path figure is the triaxial failure envelope generated from this material. Tables I, II and III give computer listings for each test. Table Column 1 gives the data point while columns 2 through 8 give confining pressure (p_c) in kilobars, axial load ($\sigma_a - p_c$) in kilobars, axial strain (ϵ_a) in percent, the two transverse strains (ϵ_{t_1} and ϵ_{t_2}) in percent, volume strain ($\epsilon_a + \epsilon_{t_1} + \epsilon_{t_2}$) in percent and mean stress [$1/3(\sigma_a + 2p_c)$] in kilobars. All plots were constructed from these tables.

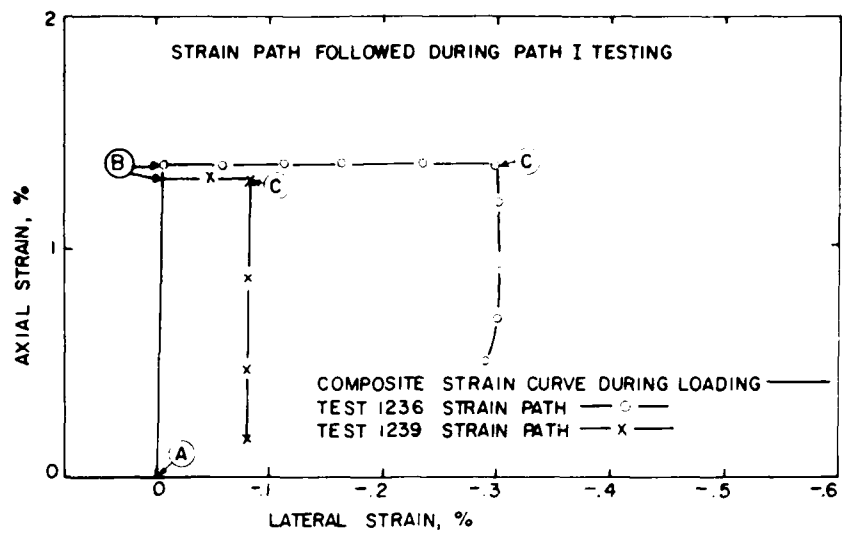


Figure 5a. Strain path followed during uniaxial-strain loading and constant-axial and uniaxial-strain unloading.

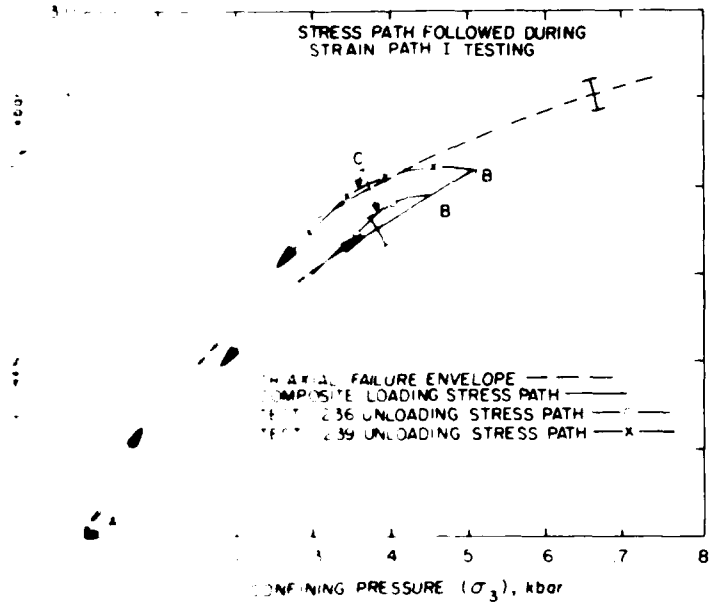


Figure 5b. Stress path followed during uniaxial-strain loading and constant-axial and uniaxial-strain unloading. The resulting stress path is a composite of four tests.

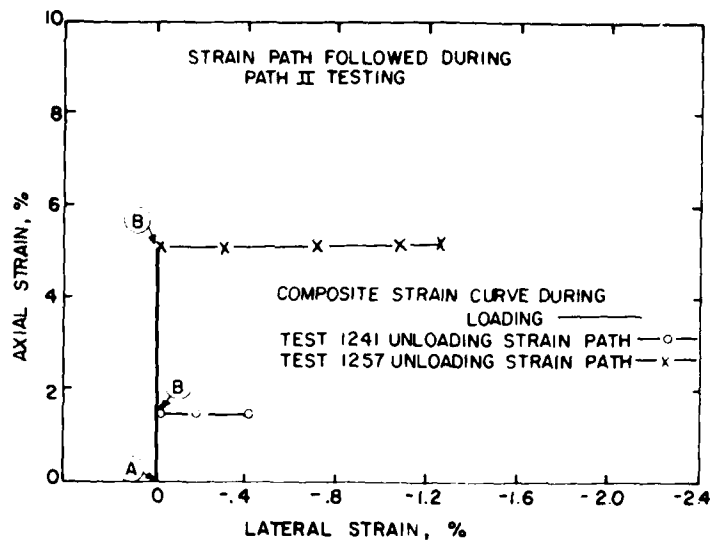


Figure 6a. Strain path followed during uniaxial-strain loading and constant-axial-strain unloading. The resulting stress path is a composite of four tests.

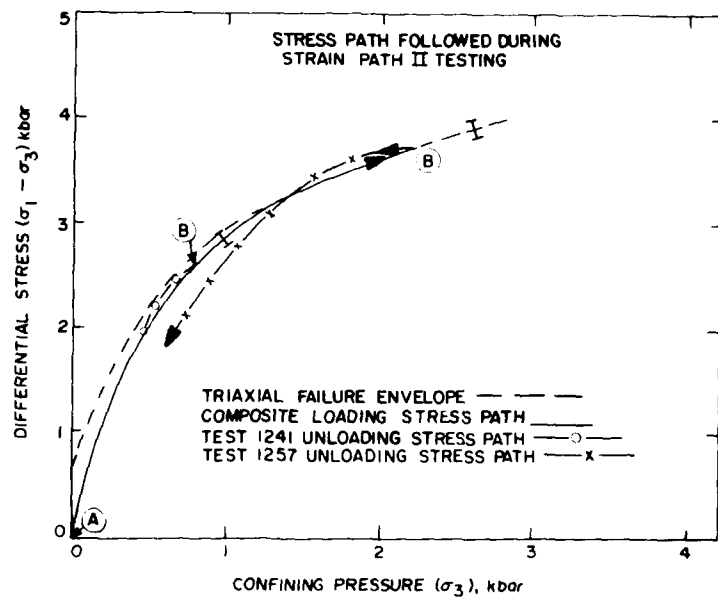


Figure 6b. Stress path followed during uniaxial-strain loading and constant-axial-strain unloading. The resulting stress path is a composite of four tests.

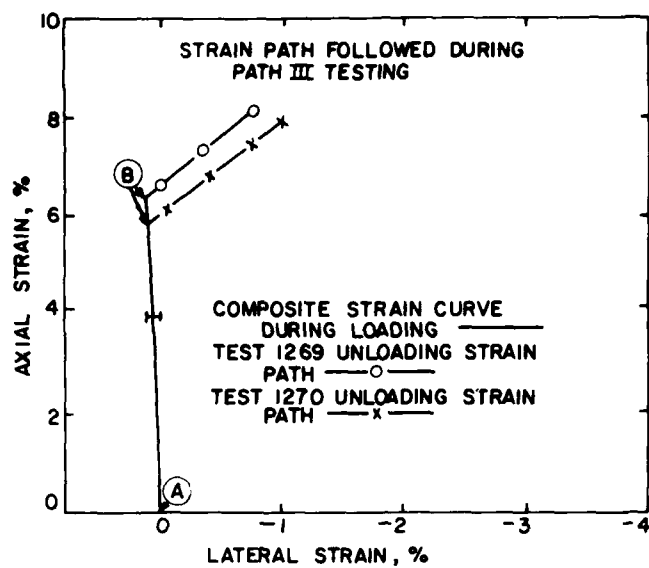


Figure 7a. Strain path followed during uniaxial-strain loading and constant-volume-strain unloading. The resulting stress path is a composite of three tests.

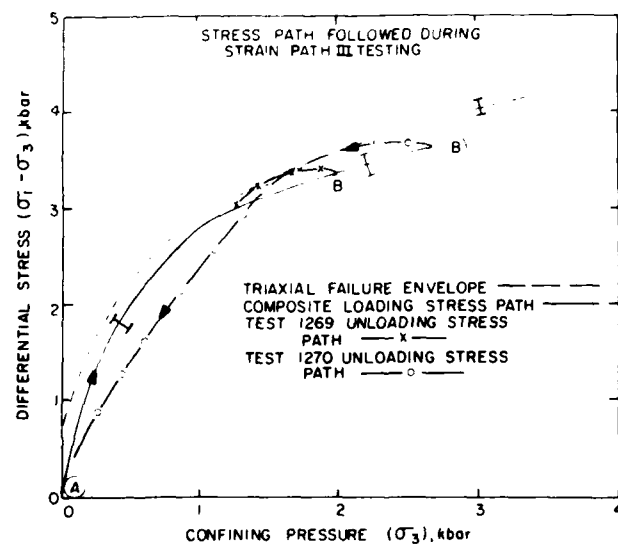


Figure 7b. Stress path followed during uniaxial-strain-loading and constant-volume-strain unloading. The resulting stress path is a composite of three tests.

TABLE Ia
1236 Test Results

Path Type I

N	PRESS (kN)	LORD (kN)	ER (λ)	ER (λ)	ET1 (λ)	ET2 (λ)	VOL STRAIN(λ)	MEAN STRESS(kN)
1	0	58974.3E-3	-	198966E-2	-227923E-2	386529E-2	-403623E-3	-196581E-3
2	83154E-2	121886	181541	289242E-1	-249537E-1	1844887	-488590E-1	12531
3	268948E-1	313389	385941E-1	311286	-399487E-1	211266	-12531	12531
4	318743E-1	477283	48812	648219	-584243E-1	397986	-199942	199942
5	595919E-1	728734	532129	515367E-1	-613672E-1	529813	-383503	383503
6	914661E-1	86485	684486	572956E-1	-687519	594491	-367277	367277
7	101246E-1	91214	633116	619889E-1	-675545E-1	62734	-395513	395513
8	161246E-1	94968	654895	632093E-1	-658088E-1	652086	-419868	419868
9	121955	1	85325	788724	654594E-1	667988E-1	797375	479871
10	148221	1	16264	641159E-1	-11111E-1	788794	532367	532367
11	173231	1	27378	862888	618403E-1	-738928E-1	813543	597826
12	134619	1	3286	862888	6154593E-1	-738928E-1	813543	597826
13	213424	1	36294	8964641	684471E-1	-682473E-1	896462	667733
14	235594	1	44655	938102	672353E-1	-702874E-1	935593	717712
15	253075	1	48258	955794	703073E-1	-687145E-1	961671	751681
16	28486	1	68682	1 051519	678841E-1	-788389E-1	1 02213	817613
17	307501	1	6397	1 05002	674118E-1	-948761E-1	1 04792	859866
18	33	1	75746	1 10718	706496E-1	-639377E-1	1 10777	913836
19	35	1	8078	1 88701	6811285E-1	-6811285E-1	858188	638886
20	363093	1	86159	1 19816	7027666E-1	-7130212E-1	798047	667733
21	39195	1	93396	1 23929	664372E-1	-716842E-1	1 19712	1 01466
22	419912	1	99876	1 27295	6911569E-1	-789275E-1	1 22116	1 06459
23	432216	1	99876	1 38434	719724E-1	-686353E-1	1 38195	1 19882
24	468417	2	82878	1 63977	671977E-1	-694227E-1	1 14468	1 14468
25	48504	2	75771	1 75112	686472E-1	-694227E-1	1 17636	1 17636
26	503086	2	12155	1 7576	686472E-1	-686472E-1	1 21018	1 21018
27	486136	2	10398	2 11445	620962E-1	-968575E-1	1 15054	967708
28	52	2	45525	2 45639	620967	-7027666E-1	1 19712	1 01466
29	443272	2	10519	2 4379	1 23929	-7130212E-1	1 22116	1 06459
30	439559	2	86814	2 39862	1 031341E-1	-122558	3509802	575112
31	424761	2	0259	2 30715	1 031341E-1	-126253	254591	1 14126
32	4264	2	0259	2 30715	-250156E-1	-161672	418388	1 09944
33	415565	2	014	2 37139	-428123E-1	-453154	674261	1 05271
34	4089	2	011	2 37139	-705626E-1	-514194	1 05271	1 05271
35	448541	1	99372	2 27429	934331E-1	-105106	1 16967	1 16967
36	43522	1	87775	2 27951	112404	-106806	324676	1 16966
37	4391	1	8627	2 25585	1415341E-1	-145341E-1	1 14451	1 14451
38	439651	1	7505	2 23227	183161	-121736	342129	781584
39	438651	1	7505	2 48675	-195652E-1	-929332E-1	822395	930646
40	438651	1	6344	2 9416	-171724E-1	-93232E-1	552252	881449
41	438651	1	55954	3 17486	-175148E-1	-898614E-1	481384	819899
42	249451	1	49645	3 49849	-899382E-1	-425346	776921	418568
43	438651	1	48317	4 8317	-152192E-1	-505223	565597	66251
44	438651	1	42482	4 6275	-198412E-1	-875477E-1	575112	613065
45	438651	1	38675	5 56193	-216182E-1	-975809E-1	616139	568722
46	438651	1	356601	5 65114	-282757E-1	-913368E-1	674136	566964
47	139571	1	38896	6 652056	-205361E-1	-886296	714227	481884
48	124726	881336	-	652056	-205361E-1	-886296	-764484	-418568
49	118175	808986	-	696156	-217146E-1	-898141	-887556	-379537
50	222815	1 3761	-	752216	-193822E-1	-865676E-1	-927449	-328513
51	136741	1 24882	-	785669	-249326E-1	-914827E-1	-982251	-3028
52	1 18675	1 48275	-	84975	-277895E-1	-943515E-1	-967858	-256687
53	1 163601	1 05114	-	91621	-261278E-1	-852149E-1	-1 02492	-284662
54	1 139571	1 05114	-	999999	-1 08915E-2	-582582E-1	-1 05489	-1 98559
55	1 124726	221945	-	1 18572	-632223	-672582E-1	-1 28468	-961552E-1

* Axial strain rezeroed for constant-axial-strain unloading.

** Lateral strains rezeroed for uniaxial-strain unloading.

TABLE Ib
1239 Test Results
Path Type I

N	PRESS (kPa)	LOAD (kN)	EA (x2)	ET1 (x2)	ET2 (x2)	VOL. STRAIN(x2)	MEAN STRESS(kPa)
0	- 56499E-3	- 266982E-2	- 2270983E-2	- 384968E-2	- 48149E-3	- 194997E-3	- 194997E-3
1	194157E-1	871552E-1	156155	259938E-1	155626	48534E-1	48534E-1
2	365577E-1	293892E-1	386155	25185E-1	25185	34022	34022
3	546868E-1	473283	415955	630774	28519E-1	417986	211621
4	676159E-1	579115	472596	385855E-1	270849E-1	47195	2683
5	827807E-1	731595	549687	266499E-1	272188E-1	548186	331236
6	113801	827876	622928	282453E-1	251397E-1	628751	408721
7	144231	113557	712471	225223E-1	284208E-1	704567	469355
8	16734	108959	747585	261122E-1	35365E-1	748267	527637
9	19485	19884	811643	244899E-1	39619E-1	813394	594197
10	214266	237673	844662	227599E-1	231705E-1	844247	626898
11	24963	306536	893465	236373E-1	244658E-1	897782	685752
12	270861	142114	951811	242518E-1	22558E-1	953429	755107
13	362797	152818	1 01615	20592E-1	22708E-1	815189	815189
14	29	332227	1 62236	176215E-1	252248E-1	1 06729	827961
15	358497	1 68145	1 1132	212688E-1	241623E-1	1 11029	916979
16	392168	75475	1 75482	216898E-1	216898E-1	1 10805	978085
17	425152	1 85241	1 22391	203977E-1	251594E-1	1 21985	1 046
18	46	20	1 25948	1 25948	223659E-1	1 26051	1 09314
19	49111	1 57146	1 3112	233089E-1	231568E-1	1 51125	1 49446
20	568986	1 95893	- 243472	024179	284392E-1	- 2476682	1 15512
21	491632	1 94234	1 94234	186361E-1	023842	- 259486	1 14966
22	481926	1 94234	248897	170467E-1	426934E-1	- 2679587	1 12977
23	437656	1 95222	244164	18922E-2	512623E-2	- 245612	1 084
24	437634	1 95222	247528	1 20732E-1	677799E-1	- 21717	1 09694
25	434664	1 94034	244151	1 27152E-1	896332E-1	- 14886	1 06144
26	332475	1 87085	246776	561056E-1	109498	- 412101	1 01609
27	268618	1 75262	263177	545585E-1	106634	- 465601	95276
28	225154	1 6171	372007	531156E-1	11259	- 532954	62256
29	11515	49117	49117	561189E-1	109981	- 566783	62121
30	636476	42397	557297	557297E-1	108176	- 614229	1 6118
31	636476	511835	494986	511111E-1	107341	- 660071	1 0176
32	636476	511835	558446	523556E-1	11267	- 722583	65439
33	23126	1 0661	624899	547296E-1	110875	- 728924	157216
34	1 7498	93921	691573	544276E-1	1105	- 855747	499971
35	1 43621	8179	732791	535685E-1	11227	- 91875	1 16364
36	113801	70111	811942	520461E-1	11141	- 361112	1 16359
37	660182	560182	90572	526137E-1	112254	- 1 01012	4 5465
38	596339E-1	489782	- 1 01419	584227E-1	114039	- 1 17692	1 93228
39	499117E-1	486624	- 1 0971	505246E-1	112486	- 1 25488	1 36326
40	762786E-1	45924684-1	- 1 38787	- 820595E-1	- 820595E-1	- 1 54786	226332E-1

* Axial strains rezeroed for constant-axial-strain unloading.

TABLE IIIa
1241 Test Results
Path Type II

N	PRESS. (kG)	LORD (kN)	ER (%)	E11 (E-1)	E12 (E-1)	VOL STRAIN (E-1)	MEAN STRESS (kN)
1	204628E-2	-115831E-1	-	442221E-2	172734E-2	-142955E-1	682267E-4
2	685171E-2	159629E-1	5.16E2	-544514E-2	-294666E-1	497523	202194E-1
3	1.7229E-1	1.7222	6.121E6	-594597E-2	-281611E-1	582801	74985E-1
4	2.72654E-1	3.41591	6.618E5	-782541E-3	-311459E-1	147733	147733
5	5.95759E-1	5.94986	6.6179E-3	-311739E-1	-311739E-1	675358	236649
6	8.3891E-1	7.11235	7.5156E-2	208558E-2	325259E-1	744666	328568
7	1.69578	8.252	8.61791	-865191E-1	-384373E-1	77828	387088
8	1.16E-1	9.41752	8.34895	591177E-2	-384373E-1	885742	442216
9	1.70225	1.17792	8.92617	-38692E-2	-279168E-1	849821	524733
10	1.95775	1.17792	9.15464	1.9581E-2	-4750.5E-1	86965	568365
11	2.26E-1	1.26715	9.66E8	1.94191E-2	-4750.5E-1	91612	649122
12	2.61229	1.39652	1.62326	-171985E-2	-4750.5E-1	281819	72653
13	3.0819	1.47579	1.65629	-839394E-2	-4750.5E-1	568181	568181
14	3.74296	1.5461	1.1044	446517E-2	-4750.5E-1	1.6712	446516
15	4.6244	1.6646	1.1342	859581E-2	-4750.5E-1	1.65486	859586
16	4.16349	6.1111	1.16135	-819044E-1	-508549E-1	1.18741	1.18741
17	4.82894	8.18294	1.18447	-844754E-1	-485506E-1	1.17651	1.05641
18	4.87794	1.9144	1.47501	-851422E-2	-4717.4E-1	1.12576	1.12576
19	5.4473	0.0621	1.88205	-7.2808E-2	-4717.4E-1	1.12576	1.12576
20	5.9244	4.88194	1.114	-4750.5E-1	-4750.5E-1	1.12576	1.12576
21	6.4784	1.15614	1.5624	-17075E-2	-4750.5E-1	1.0311	1.0311
22	6.86728	6.08156	1.1764	-894752E-2	-7.282E-1	1.29316	1.29316
23	6.91164	5.47967	1.9934	-5.47967	-4.81676E-1	1.29316	1.29316
24	7.05067	2.11226	1.41163	-10.1415E-1	-5.06560E-1	1.29316	1.29316
25	7.05067	1.49345	1.56285	-1.49345	-1.48380	1.48380	1.48380
26	7.1015	1.10154	1.47207	-1.87810E-1	-4717.4E-1	1.12576	1.12576
27	7.44744	2.58601	1.47207	-4750.5E-1	-4750.5E-1	1.12576	1.12576
28	7.44744	4.11181	1.48205	-7.2808E-2	-4750.5E-1	1.12576	1.12576
29	7.6644	4.036	1.48205	-894752E-2	-4750.5E-1	1.12576	1.12576
30	7.6644	4.43179	1.77754E-2	-656011E-1	-4.81676E-1	1.48380	1.48380
31	7.6644	4.43179	1.81775E-2	-1.87810E-1	-4.81676E-1	1.48380	1.48380
32	7.6644	4.43179	1.84431E-2	-5.11419E-1	-4.81676E-1	1.48380	1.48380
33	7.6644	4.43179	1.84431E-2	-5.11419E-1	-4.81676E-1	1.48380	1.48380
34	7.6644	4.43179	1.84431E-2	-5.11419E-1	-4.81676E-1	1.48380	1.48380
35	7.6644	4.43179	1.84431E-2	-5.11419E-1	-4.81676E-1	1.48380	1.48380
36	7.6644	4.43179	1.84431E-2	-5.11419E-1	-4.81676E-1	1.48380	1.48380
37	7.6644	4.43179	1.84431E-2	-5.11419E-1	-4.81676E-1	1.48380	1.48380
38	7.6644	4.43179	1.84431E-2	-5.11419E-1	-4.81676E-1	1.48380	1.48380
39	7.6644	4.43179	1.84431E-2	-5.11419E-1	-4.81676E-1	1.48380	1.48380
40	7.6644	4.43179	1.84431E-2	-5.11419E-1	-4.81676E-1	1.48380	1.48380
41	7.6644	4.43179	1.84431E-2	-5.11419E-1	-4.81676E-1	1.48380	1.48380
42	7.6644	4.43179	1.84431E-2	-5.11419E-1	-4.81676E-1	1.48380	1.48380
43	7.6644	4.43179	1.84431E-2	-5.11419E-1	-4.81676E-1	1.48380	1.48380
44	7.6644	4.43179	1.84431E-2	-5.11419E-1	-4.81676E-1	1.48380	1.48380
45	7.6644	4.43179	1.84431E-2	-5.11419E-1	-4.81676E-1	1.48380	1.48380
46	7.6644	4.43179	1.84431E-2	-5.11419E-1	-4.81676E-1	1.48380	1.48380
47	7.6644	4.43179	1.84431E-2	-5.11419E-1	-4.81676E-1	1.48380	1.48380
48	7.6644	4.43179	1.84431E-2	-5.11419E-1	-4.81676E-1	1.48380	1.48380
49	7.6644	4.43179	1.84431E-2	-5.11419E-1	-4.81676E-1	1.48380	1.48380
50	7.6644	4.43179	1.84431E-2	-5.11419E-1	-4.81676E-1	1.48380	1.48380
51	7.6644	4.43179	1.84431E-2	-5.11419E-1	-4.81676E-1	1.48380	1.48380
52	7.6644	4.43179	1.84431E-2	-5.11419E-1	-4.81676E-1	1.48380	1.48380
53	7.6644	4.43179	1.84431E-2	-5.11419E-1	-4.81676E-1	1.48380	1.48380
54	7.6644	4.43179	1.84431E-2	-5.11419E-1	-4.81676E-1	1.48380	1.48380
55	7.6644	4.43179	1.84431E-2	-5.11419E-1	-4.81676E-1	1.48380	1.48380
56	7.6644	4.43179	1.84431E-2	-5.11419E-1	-4.81676E-1	1.48380	1.48380
57	7.6644	4.43179	1.84431E-2	-5.11419E-1	-4.81676E-1	1.48380	1.48380
58	7.6644	4.43179	1.84431E-2	-5.11419E-1	-4.81676E-1	1.48380	1.48380
59	7.6644	4.43179	1.84431E-2	-5.11419E-1	-4.81676E-1	1.48380	1.48380
60	7.6644	4.43179	1.84431E-2	-5.11419E-1	-4.81676E-1	1.48380	1.48380
61	7.6644	4.43179	1.84431E-2	-5.11419E-1	-4.81676E-1	1.48380	1.48380
62	7.6644	4.43179	1.84431E-2	-5.11419E-1	-4.81676E-1	1.48380	1.48380
63	7.6644	4.43179	1.84431E-2	-5.11419E-1	-4.81676E-1	1.48380	1.48380
64	7.6644	4.43179	1.84431E-2	-5.11419E-1	-4.81676E-1	1.48380	1.48380
65	7.6644	4.43179	1.84431E-2	-5.11419E-1	-4.81676E-1	1.48380	1.48380
66	7.6644	4.43179	1.84431E-2	-5.11419E-1	-4.81676E-1	1.48380	1.48380
67	7.6644	4.43179	1.84431E-2	-5.11419E-1	-4.81676E-1	1.48380	1.48380
68	7.6644	4.43179	1.84431E-2	-5.11419E-1	-4.81676E-1	1.48380	1.48380
69	7.6644	4.43179	1.84431E-2	-5.11419E-1	-4.81676E-1	1.48380	1.48380
70	7.6644	4.43179	1.84431E-2	-5.11419E-1	-4.81676E-1	1.48380	1.48380
71	7.6644	4.43179	1.84431E-2	-5.11419E-1	-4.81676E-1	1.48380	1.48380
72	7.6644	4.43179	1.84431E-2	-5.11419E-1	-4.81676E-1	1.48380	1.48380
73	7.6644	4.43179	1.84431E-2	-5.11419E-1	-4.81676E-1	1.48380	1.48380
74	7.6644	4.43179	1.84431E-2	-5.11419E-1	-4.81676E-1	1.48380	1.48380
75	7.6644	4.43179	1.84431E-2	-5.11419E-1	-4.81676E-1	1.48380	1.48380
76	7.6644	4.43179	1.84431E-2	-5.11419E-1	-4.81676E-1	1.48380	1.48380
77	7.6644	4.43179	1.84431E-2	-5.11419E-1	-4.81676E-1	1.48380	1.48380
78	7.6644	4.43179	1.84431E-2	-5.11419E-1	-4.81676E-1	1.48380	1.48380
79	7.6644	4.43179	1.84431E-2	-5.11419E-1	-4.81676E-1	1.48380	1.48380
80	7.6644	4.43179	1.84431E-2	-5.11419E-1	-4.81676E-1	1.48380	1.48380
81	7.6644	4.43179	1.84431E-2	-5.11419E-1	-4.81676E-1	1.48380	1.48380
82	7.6644	4.43179	1.84431E-2	-5.11419E-1	-4.81676E-1	1.48380	1.48380
83	7.6644	4.43179	1.84431E-2	-5.11419E-1	-4.81676E-1	1.48380	1.48380
84	7.6644	4.43179	1.84431E-2	-5.11419E-1	-4.81676E-1	1.48380	1.48380
85	7.6644	4.43179	1.84431E-2	-5.11419E-1	-4.81676E-1	1.48380	1.48380
86	7.6644	4.43179	1.84431E-2	-5.11419E-1	-4.81676E-1	1.48380	1.48380
87	7.6644	4.43179	1.84431E-2	-5.11419E-1	-4.81676E-1	1.48380	1.48380
88	7.6644	4.43179	1.84431E-2	-5.11419E-1	-4.81676E-1	1.48380	1.48380
89	7.6644	4.43179	1.84431E-2	-5.11419E-1	-4.81676E-1	1.48380	1.48380
90	7.6644	4.43179	1.84431E-2	-5.11419E-1	-4.81676E-1	1.48380	1.48380
91	7.6644	4.43179	1.84431E-2	-5.11419E-1	-4.81676E-1	1.48380	1.48380
92	7.6644	4.43179	1.84431E-2	-5.11419E-1	-4.81676E-1	1.48380	1.48380
93	7.6644	4.43179	1.84431E-2	-5.11419E-1	-4.81676E-1	1.48380	1.48380
94	7.6644	4.43179	1.84431E-2	-5.11419E-1	-4.81676E-1	1.48380	1.48380
95	7.6644	4.43179	1.84431E-2	-5.11419E-1	-4.81676E-1	1.48380	1.48380
96	7.6644	4.43179	1.84431E-2	-5.11419E-1	-4.81676E-1	1.48380	1.48380
97	7.6644	4.43179	1.84431E-2	-5.11419E-1	-4.81676E-1	1.48380	1.48380
98	7.6644	4.43179	1.84431E-2	-5.11419E-1	-4.81676E-1	1.48380	1.48380
99	7.6644	4.43179	1.84431E-2	-5.11419E-1	-4.81676E-1	1.48380	1.48380
100	7.6644	4.43179	1.84431E-2	-5.11419E-1	-4.81676E-1	1.48380	1.48380
101	7.6644	4.43179	1.84431E-2	-5.11419E-1	-4.81676E-1	1.48380	1.48380
102	7.6644	4.43179	1.84431E-2	-5.11419E-1	-4.81676E-1	1.48380	1.48380
103	7.6644	4.43179	1.84431E-2	-5.11419E-1	-4.81676E-1	1.48380	1.48380
104	7.6644	4.43179	1.84431E-2	-5.11419E-1	-4.81676E-1	1.48380	1.48380
105	7.6644	4.43179	1.84431E-2	-5.11419E-1	-4.81676E-1	1.48380	1.48380
106	7.6644	4.43179	1.84431E-2	-5.11419E-1	-4.81676E-1	1.48380	1.48380
107	7.6644	4.43179	1.84431E-2	-5.11419E-1	-4		

TABLE IIb
1257 Test Results
Path Type II

N	CPRESS (kB)	LOAD (kB)	EA (x)	EA (z)	ET1 (x)	ET1 (z)	ET2 (x)	ET2 (z)	VOL STRAIN(%)	MEAN STRESS(kB)
0	-1.9868E-1	9819.5	-869649E-2	-869649E-2	-611251E-2	-624866E-2	-219496E-1	-219496E-1	-495981E-5	-452251E-1
1	363063E-1	1354	-	-	-161162E-1	-161162E-1	-116152	-116152	-116152	-116152
2	363063E-1	26764	298826	-	812948	-	738807E-2	276431	119853	119853
3	723239E-1	492886	44911	-	828544E-2	-	827474E-2	432393	232386	232386
4	201129	1 10017	793277	-	8697205	-	149653E-1	775318	567552	567552
5	387264	1 38882	984475	-	572949E-2	-	91224	965814	780144	780144
6	497313	1 87199	1 3881	-	794519E-2	-	194198E-1	1 227232	1 12131	1 12131
7	546906	1 9480	1 35269	-	391581E-2	-	169373E-1	1 33296	1 19625	1 19625
8	579969	1 4176	1 41992	-	514466E-2	-	188919E-1	1 39322	1 26228	1 26228
9	680633	2 26515	1 56354	-	389635E-2	-	821617	1 53763	1 43458	1 43458
10	725954	2 33251	1 61083	-	172212E-2	-	20350E-1	1 5835	-	-
11	-6.16189	2 40457	1 66451	-	261109E-2	-	247498E-1	1 6365	1 56471	1 56471
12	728951	2 46716	1 70425	-	189214E-2	-	248208E-1	1 67786	1 61182	1 61182
13	822736	2 56945	1 75592	-	121275E-2	-	31932E-1	1 73735	1 66429	1 66429
14	885195	2 62541	1 84435	-	632482E-2	-	261527E-1	1 81836	1 76427	1 76427
15	908459	2 71291	1 90657	-	178195E-2	-	269812E-1	1 84725	1 80882	1 80882
16	922459	2 71291	1 92109	-	211972E-2	-	272343E-1	1 87655	1 82229	1 82229
17	946599	2 71291	1 94927E-3	-	494927E-3	-	922347	1 90679	1 85215	1 85215
18	9725139	2 74789	1 96086	-	610578E-2	-	224108E-1	1 94322	1 8915	1 8915
19	1 02118	2 85386	2 042	-	256034E-2	-	262755E-1	2 0178	1 9274	1 9274
20	1 04657	2 90255	2 09426	-	116712E-2	-	252145E-1	2 06865	2 0149	2 0149
21	1 09657	2 93722	2 15461	-	251423E-2	-	222904E-1	2 13441	2 07564	2 07564
22	1 168	2 09442	2 21223	-	325846E-2	-	265805E-1	2 2806	2 1983	2 1983
23	1 20578	1 11395	2 40715	-	205711E-2	-	248868E-1	2 38058	2 24676	2 24676
24	1 24575	1 1295	2 46936	-	320668E-2	-	233135E-1	2 48217	2 28752	2 28752
25	1 28154	1 1795	2 638972	-	229194E-2	-	2206135E-1	2 65956	2 33241	2 33241
26	1 32536	1 17929	2 819887	-	721278E-2	-	181939E-1	2 81227	2 37811	2 37811
27	1 35469	1 1948	3 04567	-	111814E-1	-	183468E-1	2 91584	2 42431	2 42431
28	1 3987	1 25049	3 2567	-	779904	-	110108E-1	3 174897	2 76535	2 76535
29	1 47864	4 10846	4 10866	-	179866	-	878895E-2	4 07189	2 84266	2 84266
30	1 49552	4 10862	4 487361	-	231071E-1	-	285185E-2	4 45118	2 1172	2 1172
31	1 51247	4 10847	4 8432	-	294947E-1	-	4 81241	4 39734	-	-
32	1 52621	5 3457	5 3915	-	264155E-2	-	322872E-1	4 9885	5 54407	5 54407
33	1 53136	5 7912	5 11999	-	276415E-1	-	257692E-2	5 09343	5 65115	5 65115
34	1 56148	72947	3 35449	-	509456E-1	-	291423E-1	5 15229	5 58973	5 58973
35	1 58114	75247	2 28119	-	116933	-	977041E-1	5 54287	5 36229	5 36229
36	1 62167	71192	1 15384	-	156404	-	141204	-	61275	2 66886
37	1 71227	5647	2 91567	-	254155	-	248676	-	784345	2 96287
38	1 49612	28441	2 79394	-	487819	-	392585	-	97589	2 50899
39	986115	2 5663	2 44695	-	615422	-	722266	-	84192	1 87533
40	724616	1 32715	2 14	-	1 38836	-	-1 12775	-	70818	1 45533
41	681911	1 804	-1 161778	-	-1 11778	-	-1 194421	-	475356	1 3664

* Axial strain rezeroed for constant-axial-strain unloading.

TABLE IIIC*

1285 Test Results

Path Type II

<i>n</i>	CFR4- <i>n</i> -16	Light- <i>n</i> -16	EH- <i>n</i> -1	EH- <i>n</i> -2	EH- <i>n</i> -3	EH- <i>n</i> -4	VAL. STRAIN, %	MEAN STRESS, MPa
0	-34.825E-3	-33.8065E-2	-980323	-268726E-2	-981065E-2	-268726E-2	-127942E-3	921962E-2
1	142881E-2	232386E-1	493755E-1	6115984E-2	858556E-2	482412E-2	423919E-1	111862
2	192889E-1	275378	35834	117336E-1	118382E-1	1.7635E-2	551877	261875
3	572216E-1	627954	506816	157366E-1	267322E-1	916211E-1	576262	233337
4	743595E-1	780115	681141	212349E-1	267322E-1	916211E-1	756085	233337
5	101144E-1	891758	770669	162334E-1	651835E-1	834893	45176	238698
6	122878	986647	947272	162334E-1	789414E-2	932925	531817	238698
7	161599	136675	943892	120042E-1	421043E-2	989342	581727	683024
8	135071	119609	101532	611275	486564E-2	1 1156	81856	81856
9	125073	124395	125073	1 12542	1 1156	1 1156	1 1156	1 1156
10	19119	1 5632	1 25577	1 1156	1 1156	1 1156	1 1156	1 1156
11	403 54	1 78856	1 50611	1 1156	1 1156	1 1156	1 1156	1 1156
12	449 61	1 9678	1 61617	1 1156	1 1156	1 1156	1 1156	1 1156
13	477 927	1 96145	1 61124	1 14684E-1	784199E-2	1 6336	1 13175	1 13175
14	547 949	2 1047	1 78364	1 180318E-1	941694E-2	1 75595	1 24953	1 24953
15	610817	2 25916	1 98768	1 192315E-1	177829E-1	1 98575	1 36887	1 36887
16	67511	2 40616	2 61607	1 95538E-1	85114E-2	1 66144	1 46647	1 46647
17	7155	2 42601	2 61734	1 860773E-1	591604E-2	2 67751	1 51122	1 51122
18	782275	2 52382	2 2417	1 96129E-1	2391889E-2	2 18759	1 63228	1 63228
19	846141	2 54911	2 42679	2 227172E-1	548758E-2	2 59159	1 72044	1 72044
20	8880148	2 61771	2 52629	1 963521E-1	971152E-2	2 54157	1 77139	1 77139
21	944441	2 46722	2 46722	1 941881E-1	1 21494E-2	2 44838	1 84475	1 84475
22	9444416	2 806479	2 5619	6296E-2	1 21494E-2	2 52117	1 88594	1 88594
23	95317	2 656738	2 656738	1 575659E-1	2 656738E-1	2 656738E-1	1 94405	1 94405
24	1 0215	2 91294	2 91294	2 164981E-1	2 489087E-1	2 78795	1 58132	1 58132
25	1 0195	2 88011	2 88011	2 88011	2 141657E-1	2 863	1 99501	1 99501
26	1 08018	2 98865	2 98865	2 98865	1 653971E-2	3 10861	1 04953	1 04953
27	1 168777	2 44861	2 65916	1 151515E-1	1 516835E-4	3 68034	2 17172	2 17172
28	1 227745	1 6611	1 66108	1 151515E-1	1 938971E-1	4 14142E-2	2 84475	2 84475
29	1 0122	1 11091	1 4559	2 214288E-1	556429E-2	4 25876	2 67159	2 67159
30	1 375944	4 11974	4 14419	2 227166E-1	8689497E-2	4 34753	2 41587	2 41587
31	1 54174	4 29474	4 29474	2 977575E-1	1 12942E-1	4 96055	2 63127	2 63127
32	1 62171	5 35562	5 41754	2 213394E-1	1 28983E-1	5 28143	2 77985	2 77985
33	1 78744	3 42621	5 88727	1 76119E-1	1 33488E-1	5 8145	2 92953	2 92953
34	1 86485	4 46595	6 08285	2 81019E-1	1 25531E-1	6 65427	1 02658	1 02658
35	1 39841	5 1448	6 42119	6 194942E-1	1 258767E-1	6 44866	1 1894	1 1894
36	2 10424	6 3666	6 72226	6 194942E-1	743592E-2	6 69299	2 31752	2 31752
37	2 21027	6 72337	6 9364	1 96284E-1	6 234442E-2	6 90874	3 43483	3 43483

* Showing only the uniaxial-strain loading.

TABLE IIIa
1269 Test Results
Path Type III

N	CPFE	LWDE	PA	ET1	ET2	VUL STRAIN-X	MEAN STRESS(kB)
0	2276.36E-2	-1.273.08E-2	-8.201.44E-2	-2.296.61E-2	-9.82016E-4	-75877.3E-4	-447127E-1
1	125846	-23.7922	129875E-1	23.7922	263284E-2	24.732	664446
2	174692	285465	229375E-1	554722	585931E-2	31.915	119438
3	126142E-1	5.00852	216844E-2	405245	418729E-2	4.3344	284308
4	2762.39E-1	6.74667	257032E-1	554722	759555E-2	6.9807	269865
5	1.215.31E-1	6.60527	256479E-1	6.60527	151955E-1	7.7524	321447
6	4.76.31E-1	7.93.34	269.58E-1	7.75.9	1283.31E-1	8.55.57	268414
7	6.77.18E-1	8.02.25	2854.63E-1	8.02.25	256931E-1	9.41.69	416131
8	7.95.43E-1	8.17.42	3564.88E-1	8.66.731	366566E-1	10.83.77	476533
9	9.66.42E-1	9.66.736	31.0868E-1	9.68563	982.241E-2	9.9857	538951
10	11.48.73E-1	11.48.736	1.48575	1.48575	1.92.85E-1	1.03206	661.16
11	1.72.54	1.73.076	1.15.076	1.15.076	1.47.58E-1	1.167.76	671.14
12	1.99.4	1.99.4	1.44.4	1.44.4	1.78.5E-1	1.27.74	71.08
13	2.29.46	2.44.2	1.21.7	1.21.7	1.45.48E-1	1.45.52	77.8816
14	2.66.36E	1.5.45	1.46.11	1.46.11	1.84.475E-1	1.46.622	866.974
15	3.16.97	1.95.6	1.55.14	1.55.14	1.86.12E-1	1.62.204	866.25
16	3.71.74	1.80.54	1.72.51	1.72.51	0.91.61	0.91.74	901.867
17	4.31.03E	1.72.4	1.65.1	1.65.1	0.62.67E-1	1.03.49	922.645
18	4.91.34	1.61.7	1.54.04	1.54.04	0.52.27E-1	1.03.5	96.9568
19	5.52.06	1.51.7	1.45.01	1.45.01	0.43.949E-1	1.61.825	2.16241
20	6.11.51	1.40.04	1.34.14	1.34.14	0.34.9805E-1	1.75.39	2.746.94
21	6.70.87E	1.31.4	1.25.44	1.25.44	0.25.9305E-1	1.98.156	1.115.2
22	7.30.11	1.21.1	1.14.61	1.14.61	0.16.944E-1	2.11.1	1.7921
23	7.89.34	1.12.4	1.06.05	1.06.05	0.08.944E-1	2.41.71	4.48.71
24	8.48.14	1.02.4	9.44.04	9.44.04	0.03.0305E-1	2.22.944	2.51.292
25	9.07.32	9.12.4	8.51.10	8.51.10	0.04.20305E-1	2.12.97	2.79.77
26	9.66.20E	1.2.56	7.65.6	7.65.6	0.05.579E-1	2.6.576	2.81.645
27	1.02.12	4.05.6	6.24.44	6.24.44	0.01.0105E-1	1.42.15	1.46.942
28	1.07.42	1.01.11	1.01.11	1.01.11	0.01.0105E-1	1.42.15	1.46.942
29	1.13.12	1.13.1	1.04.64	1.04.64	0.01.0105E-1	1.14.64	2.6036
30	1.18.42	1.18.4	1.04.44	1.04.44	0.01.0105E-1	1.11.64	1.22.46
31	1.23.40E	1.23.40E	1.06.05	1.06.05	0.01.0105E-1	1.06.05	1.25.31
32	1.28.15	1.28.15	1.01.11	1.01.11	0.01.0105E-1	1.01.11	1.27.75
33	1.32.54	1.32.54	9.51.5	9.51.5	0.01.0105E-1	9.51.5	1.41.415
34	1.36.93	1.36.93	8.51.1	8.51.1	0.01.0105E-1	8.51.1	1.46.55
35	1.41.32	1.41.32	7.65.6	7.65.6	0.01.0105E-1	7.65.6	2.56.97
36	1.45.71	1.45.71	6.24.44	6.24.44	0.01.0105E-1	6.24.44	1.74.56
37	1.50.10E	2.57.6	5.20.14	5.20.14	0.01.0105E-1	5.20.14	1.81.32
38	1.54.49	2.84.15	4.18.4	4.18.4	0.01.0105E-1	4.18.4	4.66.5
39	1.58.88	2.70.67	4.17.47	4.17.47	0.01.0105E-1	4.17.47	4.29.86
40	1.63.27	2.74.47	4.16.47	4.16.47	0.01.0105E-1	4.16.47	2.12.58
41	1.67.61	1.67.61	4.15.4	4.15.4	0.01.0105E-1	4.15.4	1.87.83
42	1.72.91	1.72.91	4.14.4	4.14.4	0.01.0105E-1	4.14.4	1.75.17
43	1.77.25	1.77.25	4.13.4	4.13.4	0.01.0105E-1	4.13.4	1.32946
44	1.81.6	1.81.6	4.12.4	4.12.4	0.01.0105E-1	4.12.4	2.12.75
45	1.85.9	1.85.9	4.11.4	4.11.4	0.01.0105E-1	4.11.4	2.37.97
46	1.90.2	1.90.2	4.10.4	4.10.4	0.01.0105E-1	4.10.4	1.85.5
47	1.94.5	1.94.5	4.9.4	4.9.4	0.01.0105E-1	4.9.4	2.62.902
48	1.98.8	1.98.8	4.8.4	4.8.4	0.01.0105E-1	4.8.4	2.98.86
49	2.03.1	2.03.1	4.7.4	4.7.4	0.01.0105E-1	4.7.4	4.29.45
50	2.07.4	2.07.4	4.6.4	4.6.4	0.01.0105E-1	4.6.4	4.13.7
51	2.11.7	2.11.7	4.5.4	4.5.4	0.01.0105E-1	4.5.4	2.45.78
52	2.16.1	2.16.1	4.4.4	4.4.4	0.01.0105E-1	4.4.4	1.76.3
53	2.20.4	2.20.4	4.3.4	4.3.4	0.01.0105E-1	4.3.4	1.19.5
54	2.24.7	2.24.7	4.2.4	4.2.4	0.01.0105E-1	4.2.4	1.76.2
55	2.29.1	2.29.1	4.1.4	4.1.4	0.01.0105E-1	4.1.4	1.95.35
56	2.33.4	2.33.4	4.0.4	4.0.4	0.01.0105E-1	4.0.4	1.97.15
57	2.37.7	2.37.7	3.9.4	3.9.4	0.01.0105E-1	3.9.4	1.97.15
58	2.42.0	2.42.0	3.8.4	3.8.4	0.01.0105E-1	3.8.4	1.97.15
59	2.46.3	2.46.3	3.7.4	3.7.4	0.01.0105E-1	3.7.4	1.97.15
60	2.50.6	2.50.6	3.6.4	3.6.4	0.01.0105E-1	3.6.4	1.97.15
61	2.54.9	2.54.9	3.5.4	3.5.4	0.01.0105E-1	3.5.4	1.97.15
62	2.59.2	2.59.2	3.4.4	3.4.4	0.01.0105E-1	3.4.4	1.97.15
63	2.63.5	2.63.5	3.3.4	3.3.4	0.01.0105E-1	3.3.4	1.97.15
64	2.67.8	2.67.8	3.2.4	3.2.4	0.01.0105E-1	3.2.4	1.97.15
65	2.72.1	2.72.1	3.1.4	3.1.4	0.01.0105E-1	3.1.4	1.97.15
66	2.76.4	2.76.4	3.0.4	3.0.4	0.01.0105E-1	3.0.4	1.97.15
67	2.80.7	2.80.7	2.9.4	2.9.4	0.01.0105E-1	2.9.4	1.97.15
68	2.85.0	2.85.0	2.8.4	2.8.4	0.01.0105E-1	2.8.4	1.97.15
69	2.89.3	2.89.3	2.7.4	2.7.4	0.01.0105E-1	2.7.4	1.97.15
70	2.93.6	2.93.6	2.6.4	2.6.4	0.01.0105E-1	2.6.4	1.97.15
71	2.97.9	2.97.9	2.5.4	2.5.4	0.01.0105E-1	2.5.4	1.97.15
72	3.02.2	3.02.2	2.4.4	2.4.4	0.01.0105E-1	2.4.4	1.97.15
73	3.06.5	3.06.5	2.3.4	2.3.4	0.01.0105E-1	2.3.4	1.97.15
74	3.10.8	3.10.8	2.2.4	2.2.4	0.01.0105E-1	2.2.4	1.97.15
75	3.15.1	3.15.1	2.1.4	2.1.4	0.01.0105E-1	2.1.4	1.97.15
76	3.19.4	3.19.4	2.0.4	2.0.4	0.01.0105E-1	2.0.4	1.97.15
77	3.23.7	3.23.7	1.9.4	1.9.4	0.01.0105E-1	1.9.4	1.97.15
78	3.28.0	3.28.0	1.8.4	1.8.4	0.01.0105E-1	1.8.4	1.97.15
79	3.32.3	3.32.3	1.7.4	1.7.4	0.01.0105E-1	1.7.4	1.97.15
80	3.36.6	3.36.6	1.6.4	1.6.4	0.01.0105E-1	1.6.4	1.97.15
81	3.40.9	3.40.9	1.5.4	1.5.4	0.01.0105E-1	1.5.4	1.97.15
82	3.45.2	3.45.2	1.4.4	1.4.4	0.01.0105E-1	1.4.4	1.97.15
83	3.49.5	3.49.5	1.3.4	1.3.4	0.01.0105E-1	1.3.4	1.97.15
84	3.53.8	3.53.8	1.2.4	1.2.4	0.01.0105E-1	1.2.4	1.97.15
85	3.58.1	3.58.1	1.1.4	1.1.4	0.01.0105E-1	1.1.4	1.97.15
86	3.62.4	3.62.4	1.0.4	1.0.4	0.01.0105E-1	1.0.4	1.97.15
87	3.66.7	3.66.7	0.9.4	0.9.4	0.01.0105E-1	0.9.4	1.97.15
88	3.71.0	3.71.0	0.8.4	0.8.4	0.01.0105E-1	0.8.4	1.97.15
89	3.75.3	3.75.3	0.7.4	0.7.4	0.01.0105E-1	0.7.4	1.97.15
90	3.79.6	3.79.6	0.6.4	0.6.4	0.01.0105E-1	0.6.4	1.97.15
91	3.83.9	3.83.9	0.5.4	0.5.4	0.01.0105E-1	0.5.4	1.97.15
92	3.88.2	3.88.2	0.4.4	0.4.4	0.01.0105E-1	0.4.4	1.97.15
93	3.92.5	3.92.5	0.3.4	0.3.4	0.01.0105E-1	0.3.4	1.97.15
94	3.96.8	3.96.8	0.2.4	0.2.4	0.01.0105E-1	0.2.4	1.97.15
95	4.01.1	4.01.1	0.1.4	0.1.4	0.01.0105E-1	0.1.4	1.97.15
96	4.05.4	4.05.4	0.0.4	0.0.4	0.01.0105E-1	0.0.4	1.97.15
97	4.09.7	4.09.7	-0.1.4	-0.1.4	0.01.0105E-1	-0.1.4	1.97.15
98	4.14.0	4.14.0	-0.2.4	-0.2.4	0.01.0105E-1	-0.2.4	1.97.15
99	4.18.3	4.18.3	-0.3.4	-0.3.4	0.01.0105E-1	-0.3.4	1.97.15
100	4.22.6	4.22.6	-0.4.4	-0.4.4	0.01.0105E-1	-0.4.4	1.97.15
101	4.26.9	4.26.9	-0.5.4	-0.5.4	0.01.0105E-1	-0.5.4	1.97.15
102	4.31.2	4.31.2	-0.6.4	-0.6.4	0.01.0105E-1	-0.6.4	1.97.15
103	4.35.5	4.35.5	-0.7.4	-0.7.4	0.01.0105E-1	-0.7.4	1.97.15
104	4.39.8	4.39.8	-0.8.4	-0.8.4	0.01.0105E-1	-0.8.4	1.97.15
105	4.44.1	4.44.1	-0.9.4	-0.9.4	0.01.0105E-1	-0.9.4	1.97.15
106	4.48.4	4.48.4	-1.0.4	-1.0.4	0.01.0105E-1	-1.0.4	1.97.15
107	4.52.7	4.52.7	-1.1.4	-1.1.4	0.01.0105E-1	-1.1.4	1.97.15
108	4.57.0	4.57.0	-1.2.4	-1.2.4	0.01.0105E-1	-1.2.4	1.97.15
109	4.61.3	4.61.3	-1.3.4	-1.3.4	0.01.0105E-1	-1.3.4	1.97.15
110	4.65.6	4.65.6	-1.4.4	-1.4.4	0.01.0105E-1	-1.4.4	1.97.15
111	4.69.9	4.69.9	-1.5.4	-1.5.4	0.01.0105E-1	-1.5.4	1.97.15
112	4.74.2	4.74.2	-1.6.4	-1.6.4	0.01.0105E-1	-1.6.4	1.97.15
113	4.78.5	4.78.5	-1.7.4	-1.7.4	0.01.0105E-1</		

TABLE IIIb
1270 Test Results
Path Type III

* Axial strain zeroed for constant-volume unloading.

*** Could not maintain constant volume path beyond this point.

TABLE IIIIC*
1284 Test Results
Path Type III

N	PRESS (kN)	LONG. (kN)	EH	EH	EH	EH	EH	EH	ET1 (E11)	ET2 (E22)	ET3 (E33)	VOL. STRAIN (%)	MEAN STRESS (kN)
1	37665.5E-1	-38867.6E-2	-32622E-2	-1954.5E-1	-32321.5E-2	-26622E-2	-97512E-2	-105555E-3	-105555E-3	-293104E-1	-293104E-1	-733747	-462986E-1
2	854083E-2	622845E-1	75216	104608E-1	104608E-1	104608E-1	104608E-1	104608E-1	104608E-1	104608E-1	104608E-1	832651	93266
3	121169E-1	843139	544145	92252E-1	92252E-1	92252E-1	92252E-1	92252E-1	92252E-1	92252E-1	92252E-1	1 018513	1 16729
4	1570E-1	1 38E-1	1 03426	647815E-2	647815E-2	647815E-2	647815E-2	647815E-2	647815E-2	647815E-2	647815E-2	1 018513	208499
5	185125E-1	425561	1 041617	618446E	618446E	618446E	618446E	618446E	618446E	618446E	618446E	1 12734	24683
6	209085E-1	594618	1 26195	1 26195	1 26195	1 26195	1 26195	1 26195	1 26195	1 26195	1 26195	1 26195	242222
7	65129J	641162E-1	796742E-1	1 367	1 367	1 367	1 367	1 367	1 367	1 367	1 367	1 39251	347649
8	9	95756J	1 504169	1 504169	1 504169	1 504169	1 504169	1 504169	1 504169	1 504169	1 504169	1 504169	495228
9	1 26E-4	1 1187	1 56111	1 79098	1 79098	1 79098	1 79098	1 79098	1 79098	1 79098	1 79098	1 68443	559561
10	182159E-1	281519	1 59462	1 74511	1 74511	1 74511	1 74511	1 74511	1 74511	1 74511	1 74511	1 91774	742522
11	3678	42684	1 78685	1 95616	1 95616	1 95616	1 95616	1 95616	1 95616	1 95616	1 95616	1 95616	696938
12	42684	537151	1 97243	2 17498	2 17498	2 17498	2 17498	2 17498	2 17498	2 17498	2 17498	2 17498	1 07512
13	537151	537151	1 11787	1 3475	1 3475	1 3475	1 3475	1 3475	1 3475	1 3475	1 3475	1 3475	1 18463
14	540458E	641187	1 465	1 814	1 814	1 814	1 814	1 814	1 814	1 814	1 814	1 814	2 2661
15	640458E	640458E	1 49658	1 8611	1 8611	1 8611	1 8611	1 8611	1 8611	1 8611	1 8611	1 8611	2 12597
16	740724	740724	1 52714	1 9162	1 9162	1 9162	1 9162	1 9162	1 9162	1 9162	1 9162	1 9162	1 42231
17	740724	740724	1 9162	1 96111	1 96111	1 96111	1 96111	1 96111	1 96111	1 96111	1 96111	1 96111	2 48188
18	740724	740724	1 96111	1 96111	1 96111	1 96111	1 96111	1 96111	1 96111	1 96111	1 96111	1 96111	2 69295
19	810544	810544	1 9784	1 9814	1 9814	1 9814	1 9814	1 9814	1 9814	1 9814	1 9814	1 9814	2 6226
20	810544	810544	1 9814	1 9814	1 9814	1 9814	1 9814	1 9814	1 9814	1 9814	1 9814	1 9814	2 69871
21	810544	810544	1 9814	1 9814	1 9814	1 9814	1 9814	1 9814	1 9814	1 9814	1 9814	1 9814	2 1647
22	810544	810544	1 9814	1 9814	1 9814	1 9814	1 9814	1 9814	1 9814	1 9814	1 9814	1 9814	2 1469
23	412134	412134	1 9814	1 9814	1 9814	1 9814	1 9814	1 9814	1 9814	1 9814	1 9814	1 9814	2 38402
24	412134	412134	1 9814	1 9814	1 9814	1 9814	1 9814	1 9814	1 9814	1 9814	1 9814	1 9814	2 88805
25	412134	412134	1 9814	1 9814	1 9814	1 9814	1 9814	1 9814	1 9814	1 9814	1 9814	1 9814	2 88829
26	412134	412134	1 9814	1 9814	1 9814	1 9814	1 9814	1 9814	1 9814	1 9814	1 9814	1 9814	2 92771
27	412134	412134	1 9814	1 9814	1 9814	1 9814	1 9814	1 9814	1 9814	1 9814	1 9814	1 9814	3 1175
28	412134	412134	1 9814	1 9814	1 9814	1 9814	1 9814	1 9814	1 9814	1 9814	1 9814	1 9814	3 18229
29	412134	412134	1 9814	1 9814	1 9814	1 9814	1 9814	1 9814	1 9814	1 9814	1 9814	1 9814	3 4683
30	412134	412134	1 9814	1 9814	1 9814	1 9814	1 9814	1 9814	1 9814	1 9814	1 9814	1 9814	3 5681
31	412134	412134	1 9814	1 9814	1 9814	1 9814	1 9814	1 9814	1 9814	1 9814	1 9814	1 9814	2 7792
32	412134	412134	1 9814	1 9814	1 9814	1 9814	1 9814	1 9814	1 9814	1 9814	1 9814	1 9814	2 7792
33	412134	412134	1 9814	1 9814	1 9814	1 9814	1 9814	1 9814	1 9814	1 9814	1 9814	1 9814	2 7792
34	412134	412134	1 9814	1 9814	1 9814	1 9814	1 9814	1 9814	1 9814	1 9814	1 9814	1 9814	2 7792
35	412134	412134	1 9814	1 9814	1 9814	1 9814	1 9814	1 9814	1 9814	1 9814	1 9814	1 9814	2 7792
36	412134	412134	1 9814	1 9814	1 9814	1 9814	1 9814	1 9814	1 9814	1 9814	1 9814	1 9814	2 7792
37	412134	412134	1 9814	1 9814	1 9814	1 9814	1 9814	1 9814	1 9814	1 9814	1 9814	1 9814	2 7792
38	412134	412134	1 9814	1 9814	1 9814	1 9814	1 9814	1 9814	1 9814	1 9814	1 9814	1 9814	2 7792
39	412134	412134	1 9814	1 9814	1 9814	1 9814	1 9814	1 9814	1 9814	1 9814	1 9814	1 9814	2 7792
40	412134	412134	1 9814	1 9814	1 9814	1 9814	1 9814	1 9814	1 9814	1 9814	1 9814	1 9814	2 7792
41	412134	412134	1 9814	1 9814	1 9814	1 9814	1 9814	1 9814	1 9814	1 9814	1 9814	1 9814	2 7792
42	412134	412134	1 9814	1 9814	1 9814	1 9814	1 9814	1 9814	1 9814	1 9814	1 9814	1 9814	2 7792
43	412134	412134	1 9814	1 9814	1 9814	1 9814	1 9814	1 9814	1 9814	1 9814	1 9814	1 9814	2 7792
44	412134	412134	1 9814	1 9814	1 9814	1 9814	1 9814	1 9814	1 9814	1 9814	1 9814	1 9814	2 7792
45	412134	412134	1 9814	1 9814	1 9814	1 9814	1 9814	1 9814	1 9814	1 9814	1 9814	1 9814	2 7792
46	412134	412134	1 9814	1 9814	1 9814	1 9814	1 9814	1 9814	1 9814	1 9814	1 9814	1 9814	2 7792
47	412134	412134	1 9814	1 9814	1 9814	1 9814	1 9814	1 9814	1 9814	1 9814	1 9814	1 9814	2 7792
48	412134	412134	1 9814	1 9814	1 9814	1 9814	1 9814	1 9814	1 9814	1 9814	1 9814	1 9814	2 7792
49	412134	412134	1 9814	1 9814	1 9814	1 9814	1 9814	1 9814	1 9814	1 9814	1 9814	1 9814	2 7792
50	412134	412134	1 9814	1 9814	1 9814	1 9814	1 9814	1 9814	1 9814	1 9814	1 9814	1 9814	2 7792
51	412134	412134	1 9814	1 9814	1 9814	1 9814	1 9814	1 9814	1 9814	1 9814	1 9814	1 9814	2 7792
52	412134	412134	1 9814	1 9814	1 9814	1 9814	1 9814	1 9814	1 9814	1 9814	1 9814	1 9814	2 7792
53	412134	412134	1 9814	1 9814	1 9814	1 9814	1 9814	1 9814	1 9814	1 9814	1 9814	1 9814	2 7792
54	412134	412134	1 9814	1 9814	1 9814	1 9814	1 9814	1 9814	1 9814	1 9814	1 9814	1 9814	2 7792
55	412134	412134	1 9814	1 9814	1 9814	1 9814	1 9814	1 9814	1 9814	1 9814	1 9814	1 9814	2 7792
56	412134	412134	1 9814	1 9814	1 9814	1 9814	1 9814	1 9814	1 9814	1 9814	1 9814	1 9814	2 7792
57	412134	412134	1 9814	1 9814	1 9814	1 9814	1 9814	1 9814	1 9814	1 9814	1 9814	1 9814	2 7792
58	412134	412134	1 9814	1 9814	1 9814	1 9814	1 9814	1 9814	1 9814	1 9814	1 9814	1 9814	2 7792
59	412134	412134	1 9814	1 9814	1 9814	1 9814	1 9814	1 9814	1 9814	1 9814	1 9814	1 9814	2 7792
60	412134	412134	1 9814	1 9814	1 9814	1 9814	1 9814	1 9814	1 9814	1 9814	1 9814	1 9814	2 7792
61	412134	412134	1 9814	1 9814	1 9814	1 9814	1 9814	1 9814	1 9814	1 9814	1 9814	1 9814	2 7792
62	412134	412134	1 9814	1 9814	1 9814	1 9814	1 9814	1 9814	1 9814	1 9814	1 9814	1 9814	2 7792
63	412134	412134	1 9814	1 9814	1 9814	1 9814	1 9814	1 9814	1 9814	1 9814	1 9814	1 9814	2 7792
64	412134	412134	1 9814	1 9814	1 9814	1 9814	1 9814	1 9814	1 9814	1 9814	1 9814	1 9814	2 7792
65	412134	412134	1 9814	1 9814	1 9814	1 9814	1 9814	1 9814	1 9814	1 9814	1 9814	1 9814	2 7792
66	412134	412134	1 9814	1 9814	1 9814	1 9814	1 9814	1 9814	1 9814	1 9814	1 9814	1 9814	2 7792
67	412134	412134	1 9814	1 9814	1 9814	1 9814	1 9814	1 9814	1 9814	1 9814	1 9814	1 9814	2 7792
68	412134	412134	1 9814	1 9814	1 9814	1 9814	1 9814	1 9814	1 9814	1 9814	1 9814	1 9814	2 7792
69	412134	412134	1 9814	1 9814									

DISCUSSION AND CONCLUSIONS

An initial observation of the experimentally observed stresses indicates that there is little difference between the load-unload paths for strain path types II and III. Figures 6b and 7b suggest that if the yield condition is reached during uniaxial-strain loading with the stress paths following along the yield surface, then the unloading stress paths are similar in direction and magnitude for either constant-axial-strain or constant-volume-strain unloading. The numerical analysis solutions agree with the above observation in that regardless of the strain path, the stress path would follow along the yield surface during unloading (provided that yield was reached during uniaxial-strain loading). All of the experimentally observed stress paths show the unloading curve to go initially above and then cross through and go below the loading curve. The experimental unloading curves did not remain on or intersect (as in the case of strain path 2) the yield surface as illustrated by the numerical analysis.

Such variations in unloading material behavior may be modeled by including additional phenomena into the constitutive equations. Phenomena to be included in the equations would be permanent volume compaction and work-hardening of the shear failure envelope. The former effect will mainly influence the strain paths and the latter will change the stress paths, particularly in the unloading portion. It was experimentally determined that the material behaved nonlinearly during initial loading as compared to the linear model used in the numerical analysis. Such nonlinearities may be also handled by the aforementioned considerations. The observation that the unloading path lies below the loading path in stress space may be related to fracture and the resulting loss of cohesion, rather than ductile plastic flow, as assumed in the calculations.

Inclusion of pore pressure effects into the model would be of interest in future work. Both the calculations and laboratory strain-path tests should be performed under various saturation conditions. Much of the previous theoretical work, including the finite-difference computer code, already contains this capability; it has just not been exercised yet. Also of future interest would be some theoretical results for two-dimensional dynamic loading situations, expressed in terms of ϵ_a , ϵ_t , L and p_c . This could be done by calculating the following invariants as functions of time at a particular material element:

$$\tau(t) = \left\{ (1/6)[(\sigma_{11}-\sigma_{22})^2 + (\sigma_{22}-\sigma_{33})^2 + (\sigma_{33}-\sigma_{11})^2] + \sigma_{12}^2 + \sigma_{13}^2 + \sigma_{23}^2 \right\}^{1/2}, \quad (14)$$

$$p(t) = (\sigma_{11} + \sigma_{22} + \sigma_{33})/3, \quad (15)$$

$$\epsilon_v(t) = \epsilon_{11} + \epsilon_{22} + \epsilon_{33}, \quad (16)$$

$$\epsilon_d(t) = \left\{ (1/6)[(\epsilon_{11}-\epsilon_{22})^2 + (\epsilon_{22}-\epsilon_{33})^2 + (\epsilon_{33}-\epsilon_{11})^2] + \epsilon_{12}^2 + \epsilon_{13}^2 + \epsilon_{23}^2 \right\}^{1/2}. \quad (17)$$

The desired quantities used for comparison with laboratory tests are then obtained from Eqs. (9) - (12).

The results presented here have shown that

- (1) We can define strain paths for static testing of rock (and soil) samples that are more representative of actual field situations than those commonly used heretofore in constitutive modeling, and that
- (2) It is possible to reproduce these paths in laboratory tests.

APPENDIX I

General Relationships and Finite-Difference Calculations

The equation for momentum conservation in Eulerian coordinates is given by

$$-\dot{\rho} \dot{v} = \frac{\partial \sigma_r}{\partial r} + (g-1) \frac{\sigma_r - \sigma_\theta}{r} , \quad (18)$$

where ρ is the material density, v is the radial particle velocity, σ_r and σ_θ are the radial and tangential stress components, and g is 1 (for plane flow), 2 (for cylindrical flow) or 3 (for spherical flow). A dot over a variable indicates time differentiation at a fixed material element and r is the Eulerian spatial coordinate. It is inconvenient to deal with Eulerian coordinates, hence we choose to express Eq. (18) in terms of Lagrangian coordinates representing the initial configuration. We define R as the initial radial coordinate of a material element whose current radial location is at r . Radial and transverse stress components in the initial configuration (Lagrangian) are denoted σ_R and σ_θ . If the initial density is given by ρ_0 , then mass conservation requires that

$$\rho_0 R^{g-1} dR = \rho r^{g-1} dr . \quad (19)$$

If the forces on a material element are to be the same in the two representations, then

$$R^{g-1} \sigma_R = r^{g-1} \sigma_r , \quad (20)$$

$$\sigma_0 dR^{g-1} = \sigma_\theta dr^{g-1} . \quad (21)$$

Now write Eq. (18) as

$$-\rho r^{g-1} dr \dot{v} = d(r^{g-1} \sigma_r) - \sigma_\theta dr^{g-1} , \quad (22)$$

keeping in mind that the differentials on the right-hand side are taken at constant time. Substitution of Eqs. (19) - (21) into Eq. (22) then gives

$$-\rho_0 R^{g-1} dR \dot{v} = d(R^{g-1} \sigma_R) - \sigma_\theta dR^{g-1} , \quad (23)$$

or

$$-\rho_0 \dot{v} = \frac{\partial \sigma_R}{\partial R} + (g-1) \frac{\sigma_R - \sigma_\theta}{R} , \quad (24)$$

in Lagrangian coordinates.

In order to use Eq. (24) in a finite-difference solution, an artificial viscous stress q is included. The following equations, with the addition of a constitutive law, then form the basis of the numerical calculations:

$$\rho_0 \dot{v} = \frac{\partial \sigma_R}{\partial R} - (g-1) \frac{(\sigma_R - \sigma_\theta)}{R} - \frac{\partial q}{\partial R} \quad (25)$$

$$q = \rho_0 A^2 (\Delta R)^2 \left| \frac{\partial v}{\partial R} \right|^2 , \quad \frac{\partial v}{\partial R} \leq 0 \quad (26)$$

$$= 0 , \quad \frac{\partial v}{\partial R} > 0$$

$$\dot{\epsilon}_R = - \frac{\partial v}{\partial R} , \quad \dot{\epsilon}_\theta = - \frac{v}{R} , \quad (27)$$

where A is nondimensional constant on the order of unity, ΔR is the spatial increment in the finite-difference solution, and $\dot{\epsilon}_R$ and $\dot{\epsilon}_\theta$ are the radial and tangential strain rates in the initial configuration. A straight-forward centered difference scheme is used and Eqs. (25) - (27) are written in

finite-difference form as

$$\begin{aligned}
 \rho_0 \frac{v_j^{i+\frac{1}{2}} - v_j^{i-\frac{1}{2}}}{\Delta t} &= - \frac{(\sigma_R)_{j+\frac{1}{2}}^i - (\sigma_R)_{j-\frac{1}{2}}^i}{\Delta R} - \\
 (g-1) \frac{(\sigma_R)_{j+\frac{1}{2}}^i + (\sigma_R)_{j-\frac{1}{2}}^i - (\sigma_\theta)_{j+\frac{1}{2}}^i - (\sigma_\theta)_{j-\frac{1}{2}}^i}{2R_j} \\
 &- \frac{q_{j+\frac{1}{2}}^{i-\frac{1}{2}} - q_{j-\frac{1}{2}}^{i-\frac{1}{2}}}{\Delta R}, \quad (28)
 \end{aligned}$$

$$(\dot{\varepsilon}_R)_{j+\frac{1}{2}}^{i+\frac{1}{2}} = \frac{v_j^{i+\frac{1}{2}} - v_{j+1}^{i+\frac{1}{2}}}{\Delta R}, \quad (29)$$

$$(\dot{\varepsilon}_\theta)_{j+\frac{1}{2}}^{i+\frac{1}{2}} = - \frac{v_j^{i+\frac{1}{2}} + v_{j+1}^{i+\frac{1}{2}}}{2R_{j+\frac{1}{2}}} \quad (30)$$

The stress rates ($\dot{\sigma}_R$ and $\dot{\sigma}_\theta$) are obtained from $\dot{\varepsilon}_R$ and $\dot{\varepsilon}_\theta$, and therefore the stresses and strains are calculated from

$$x_{j+\frac{1}{2}}^{i+1} = x_{j+\frac{1}{2}}^i + \dot{x}_{j+\frac{1}{2}}^{i+\frac{1}{2}} \Delta t, \quad (31)$$

where X represents σ_R , σ_θ , ε_R and ε_θ .

The constitutive model used here is expressed in terms of the principal stress and strain components σ_i and ε_i ($i = 1, 2$ and 3) with the following identification:

$g = 1$ (Plane Flow):

$$\dot{\epsilon}_1 = -\partial v / \partial R, \quad \dot{\epsilon}_2 = \dot{\epsilon}_3 = 0$$

$$\sigma_1 = \sigma_R, \quad \sigma_2 = \sigma_3 = \sigma_Z$$

$g = 2$ (Cylindrical Flow)

$$\dot{\epsilon}_1 = -\partial v / \partial R, \quad \dot{\epsilon}_2 = -v/R, \quad \dot{\epsilon}_3 = 0$$

$$\sigma_1 = \sigma_R, \quad \sigma_2 = \sigma_\theta, \quad \sigma_3 = \sigma_Z$$

$g = 3$ (Spherical Flow):

$$\dot{\epsilon}_1 = -\partial v / \partial R, \quad \dot{\epsilon}_2 = \dot{\epsilon}_3 = -v/R$$

$$\sigma_1 = \sigma_R, \quad \sigma_2 = \sigma_3 = \sigma_\theta.$$

Let us define the volume strain ϵ_V , the mean stress p , the stress deviators s_i and the second invariant of the stress tensor according to

$$\epsilon_V = \epsilon_1 + \epsilon_2 + \epsilon_3, \quad (32)$$

$$p = (\sigma_1 + \sigma_2 + \sigma_3)/3, \quad (33)$$

$$s_i = \sigma_i - p, \quad (34)$$

$$J_2 = (s_1^2 + s_2^2 + s_3^2)/2. \quad (35)$$

The elastic-plastic constitutive relation used here is then defined according to the following equations:

$$p = \hat{p}(\epsilon_v) , \quad (36)$$

$$\dot{s}_i = 2\mu(\dot{\epsilon}_i - \dot{\epsilon}_v/3) - 2\mu\xi \frac{s_i}{\sqrt{J_2}} . \quad (37)$$

The variable ξ is determined by the condition that the stress state must remain on the failure surface, defined by

$$\sqrt{J_2} = f(p) , \quad (38)$$

when a material element is undergoing plastic deformation.

From Eq. (35) we find that

$$2\sqrt{J_2} \dot{\sqrt{J_2}} = s_i \dot{s}_i \quad (\text{Summation}) \quad (39)$$

and

$$\dot{\sqrt{J_2}} = (\mu/\sqrt{J_2}) s_i \dot{\epsilon}_i - 2\mu\xi = f'(p) \dot{p} . \quad (40)$$

Therefore, the variable ξ in Eq. (37) is given by

$$2\mu\xi = (\mu/\sqrt{J_2}) s_i \dot{\epsilon}_i - f'(p) \dot{p} , \quad (41)$$

or, in terms of σ_i and p , as

$$2\mu\xi = (\mu/\sqrt{J_2})(\sigma_i \dot{\epsilon}_i - p \dot{\epsilon}_v) - f'(p) \dot{p} . \quad (42)$$

If it is desired to include effects of fluid saturation defined by nonzero pore pressure p_p , σ_i is replaced by the effective stress components $\langle\sigma_i\rangle \equiv \sigma_i - n p_p$ ($0 < n < 1$) in the elasticity relationship and by $\sigma_i^* \equiv \sigma_i - p_p$ in the failure surface relationship:

$$\langle p \rangle = p - n p_p = \hat{p}(\epsilon_v) , \quad (43)$$

$$\dot{s}_i = \dot{s}_i = 2\mu(\dot{\epsilon}_i - \dot{\epsilon}_v/3) - 2\mu\xi \frac{s_i}{\sqrt{J_2}} , \quad (44)$$

$$2\mu\xi = (\mu/\sqrt{J_2})(\sigma_i \dot{\epsilon}_i - p \dot{\epsilon}_v) - f'(p^*)(1-m)\dot{p} , \quad (45)$$

where

$$m = \frac{dp}{dp} . \quad (46)$$

The function $f(p)$ is taken to be of the form

$$f(p) = S_0 + \Delta S(1 - e^{-p/a}) . \quad (47)$$

Analytical Determination of Elastic Stress and Strain Paths for a Spherical Explosion

If $u(r,t)$ is the radial displacement, the spherical wave equation for purely elastic deformation can be written as

$$\frac{\partial^2 u}{\partial t^2} = c^2 \left[\frac{\partial^2 u}{\partial r^2} + \left(\frac{2}{r} \right) \frac{\partial u}{\partial r} - \left(\frac{2}{r^2} \right) u \right] , \quad (48)$$

where r is the radial coordinate, t is the time and c is the longitudinal elastic wave speed. This expression takes a simpler form if it is written in terms of a displacement potential ψ such that

$$u(r,t) = c^2 \frac{\partial}{\partial r} \left(\frac{\psi}{r} \right) . \quad (49)$$

In this case

$$\frac{\partial^2 \psi}{\partial t^2} = c^2 \frac{\partial^2 \psi}{\partial r^2} , \quad (50)$$

whose solution for outgoing waves is given by the familiar expression

$$\psi = \psi \left(t - \frac{r - r_0}{c} \right) . \quad (51)$$

The displacement, strain components and stress components can be expressed in terms of ψ and its derivatives ψ' and ψ'' according to

$$u(r,t) = -(c/r)\psi' - (c/r)^2 \psi , \quad (52)$$

$$-\varepsilon_a = \partial u / \partial r = (1/r)\psi'' + (2c/r^2)\psi' + (2c^2/r^3)\psi , \quad (53)$$

$$-\varepsilon_t = u/r = -(c/r^2)\psi' - (c^2/r^3)\psi , \quad (54)$$

$$-\sigma_a = (1/r) [(\lambda+2\mu)\psi'' + (4\mu c/r)\psi' + (4\mu c^2/r^2)\psi] , \quad (55)$$

$$-\sigma_t = (1/r) [\lambda\psi'' - (2\mu c/r)\psi' - (2\mu c^2/r^2)\psi] , \quad (56)$$

where λ and μ are the Lame constants. The sign convention used throughout this work is that stresses and strains are positive in compression. For a pressure history at $r = r_0$ given by

$$\left. \begin{array}{l} \sigma_r(r_0, t) = 0 \quad , \quad t < 0 \\ \sigma_r(r_0, t) = p_0 e^{-\alpha t} \quad , \quad t \geq 0 \end{array} \right\} \quad (57)$$

The function ψ must satisfy the following ordinary differential equation:

$$(\lambda+2\mu)\psi''(t) + (4\mu c/r_0)\psi'(t) + (4\mu c^2/r_0^2)\psi(t) = \quad (58)$$

$$-r_0 p_0 e^{-\alpha t} ,$$

subject to the conditions, from Eqs. (52) and (58), that jumps in ψ and ψ' at $t = 0$ obey the following relationships:

$$\begin{aligned} (\lambda + 2\mu) [\psi'] + (4\mu c/r_0) [\psi] &= 0 \quad , \\ [\psi'] + (c/r_0) [\psi] &= 0 \quad , \end{aligned} \quad (59)$$

where [] indicates the jump in the function, i.e., $[f] = f(0^+) - f(0^-)$.

Equations (59) thus require that ψ and ψ' each be continuous at $t = 0$ as long as $\lambda \neq 2\mu$. Hence, a solution to Eq. (58) can be written as

$$\psi(t) = e^{-\beta_2 t} (M \cos \beta_1 t + N \sin \beta_1 t) + \psi_0 e^{-\alpha t}, \quad (60)$$

where

$$M = -\psi_0 = \frac{r_0 p_0}{\alpha^2(\lambda+2\mu) - 4\mu c \alpha / r_0 + 4\mu c^2 / r_0^2}, \quad (61)$$

$$N = \frac{\alpha r_0 (\lambda+2\mu) - 2\mu c}{2c \sqrt{\mu(\lambda+\mu)}} \psi_0, \quad (62)$$

$$\beta_1 = \frac{2c \sqrt{\mu(\lambda+\mu)}}{r_0 (\lambda+2\mu)}, \quad (63)$$

$$\beta_2 = \frac{2\mu c}{r_0 (\lambda+2\mu)}. \quad (64)$$

In the case of an elastic fluid $\mu = 0$ and the displacement potential and its first two derivatives become

$$\psi = \frac{r_0 p_0}{\lambda \alpha^2} (1 - e^{-\alpha t} - \alpha t), \quad (65)$$

$$\psi' = \frac{r_0 p_0}{\lambda \alpha} (e^{-\alpha t} - 1), \quad (66)$$

$$\psi'' = -\frac{r_0 p_0}{\lambda} e^{-\alpha t}. \quad (67)$$

If $\alpha = 0$ (i.e., the cavity pressure remains constant at p_0) in the case of

a fluid, the displacement potential and its first two derivatives become

$$\psi = -\frac{r_0 p_0}{2\lambda} t^2 , \quad (68)$$

$$\psi' = -\frac{r_0 p_0}{\lambda} t , \quad (69)$$

$$\psi'' = -\frac{r_0 p_0}{\lambda} . \quad (70)$$

In the special case of spherical wave propagation we can make the identification that $L = \sigma_a - \sigma_t$ and $p_c = \sigma_t$, in which case the stress and strain paths can be written parametrically as

$$L = -(2\mu/r)[\psi'' + (3c/r)\psi' + (3c^2/r^2)\psi] , \quad (71)$$

$$p_c = -(1/r)[\lambda\psi'' - (2\mu c/r)\psi' - (2\mu c^2/r^2)\psi] , \quad (72)$$

$$\epsilon_a = -(1/r)[\psi'' + (2c/r)\psi' + (2c^2/r^2)\psi] , \quad (73)$$

$$\epsilon_t = (c/r^2)[\psi' + (c/r)\psi] . \quad (74)$$

Equations (71) to (74) in the case of spherical elastic waves are the analytical counterparts of Eqs. (9) to (12) for numerical solutions. Comparison of strain and stress paths calculated by the two methods is shown in Figure 8 for $1/\alpha = 1$ msec, $R/R_0 = 3$, $K = 95$ kbar, $c = 3$ km/sec, and $\rho_0 = 2.0$ gm/cm³. It can be seen that the numerical solution gives a good approximation of the strain and stress paths except for the peak values associated with the main compressive fronts. This is a result of the viscous stresses that are included in the finite-difference solution to

damp out numerical oscillations, and has no significance with regard to the conclusions reached in this report.

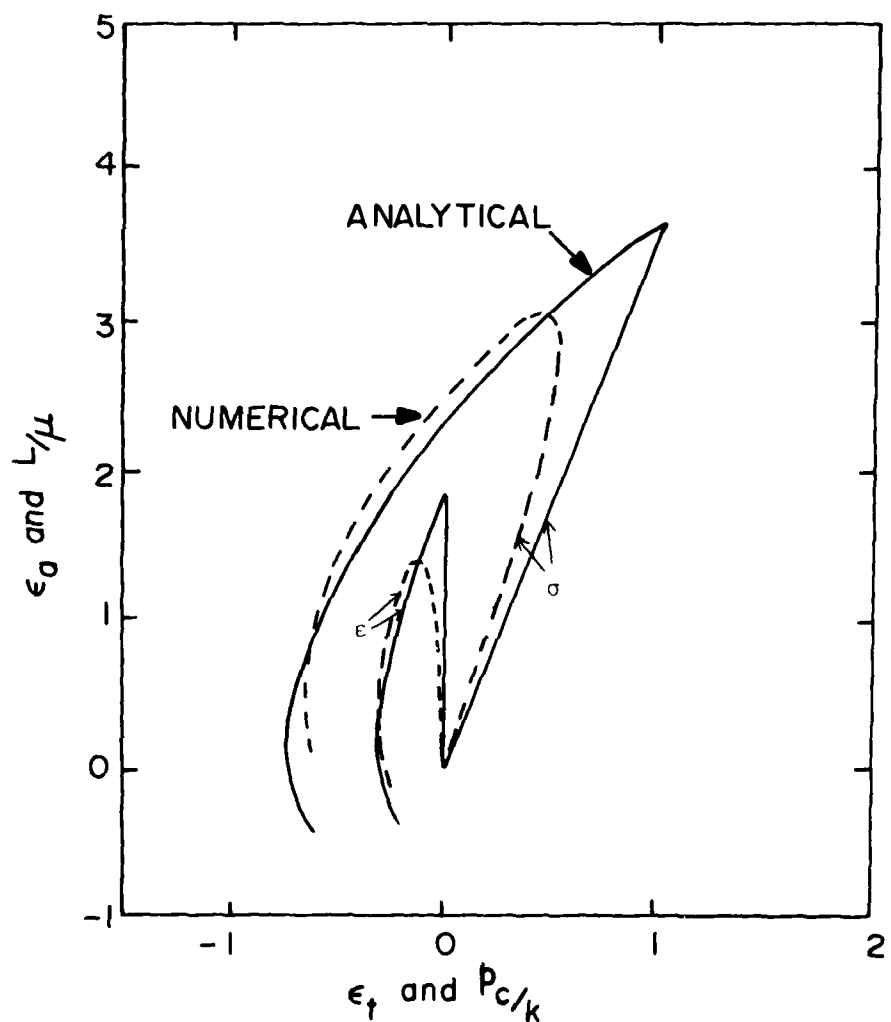


Figure 8. Comparison of strain and stress paths determined numerically and analytically for spherical wave propagation in an elastic medium.

APPENDIX II

EXPERIMENTAL TECHNIQUE

Specimen Preparation

Specimens were prepared from Kayenta sandstone, Mixed Company Site. Cylindrical samples 3.81 centimeters long by 1.91 centimeters diameter were used thus maintaining a length to diameter ratio of 2 to 1. Specimen ends were ground parallel to within $\pm .001$ centimeters. Specimens were air dried with weight, length and diameters being recorded for each sample for use in determining sample density and strains. Samples were prepared for testing by first wrapping them in urethane plastic (.025 cm thick) with hardened steel endcaps attached at each end using stainless steel lock wire.

Stress and Strain Determination

Stress and strain transducers were placed within the pressure vessel. Confining pressure was measured using a calibrated 350-ohm manganin pressure sensitive coil accurate to $\pm .003$ kbars. Jacketed samples were placed and centered on the load cell when in the pressure vessel. The load cell was accurate to $\pm .005$ kbars. Axial and lateral strain transducers were of the cantilever type using strain gauges in a wheatstone bridge configuration to obtain voltage output. The axial cantilevers measured total axial displacement and were calibrated to be accurate to $\pm .003$ percent strain. Lateral strain cantilevers were positioned at mid-sample and sampled strains at 90 degree intervals. Diametrically opposed arms were calibrated for lateral strain. The lateral strains were averages with a resulting accuracy of $\pm .006$

percent. Figure 9 shows a schematic of the transducers when inside the pressure vessel. Further discussion on transducer design may be obtained in Terra Tek report TR 75-29.

Testing Procedures

Seven samples were first tested triaxially to failure to generate the triaxial failure envelope for the material while eight samples were tested following the three strain paths. Triaxial testing commenced by first hydrostatically loading the samples to the desired confining pressure with subsequent axial loading to failure, stresses and strains being recorded during all phases of loading. A strain rate of about 10^{-4} sec⁻¹ was used during loading.

Uniaxial-strain loading was used when following a specified strain path. Axial load and confining pressure were applied such that zero lateral strain was maintained. When following strain path I, II or III during unloading, i.e., constant-axial-strain and uniaxial-strain unloading, constant axial strain unloading and constant volume strain unloading, respectively, the confining pressure and axial load were adjusted to maintain the desired strain state.

Data Acquisition and Analysis

Both x-y recorders and a PDP Lab 11 computer were used for data acquisition. The x-y recorders were used primarily for instantaneous feedback during testing while the PDP Lab 11 computer data was used for analysis of pressure effects, endcap effects and generation of stress and strain load-unload curves. Tables I, II and III presented in the text are a result of the computer analysis.

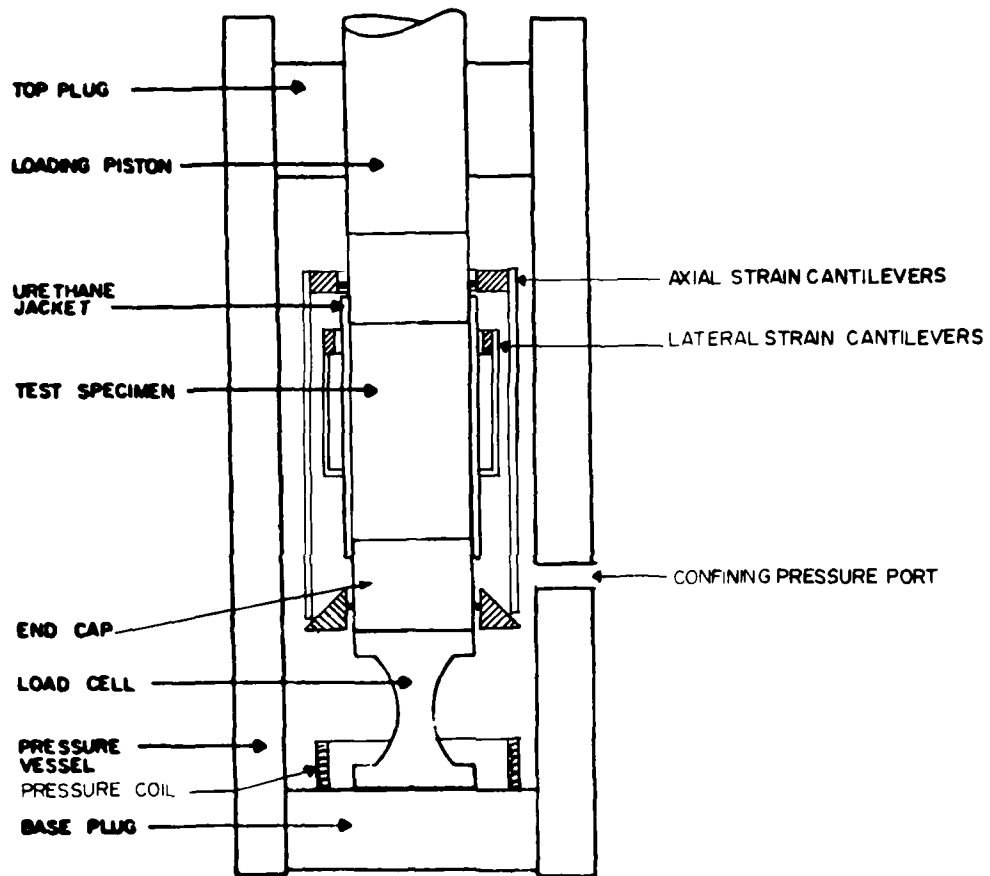


Figure 9. Pressure vessel schematic showing the sample and stress and strain transducers.

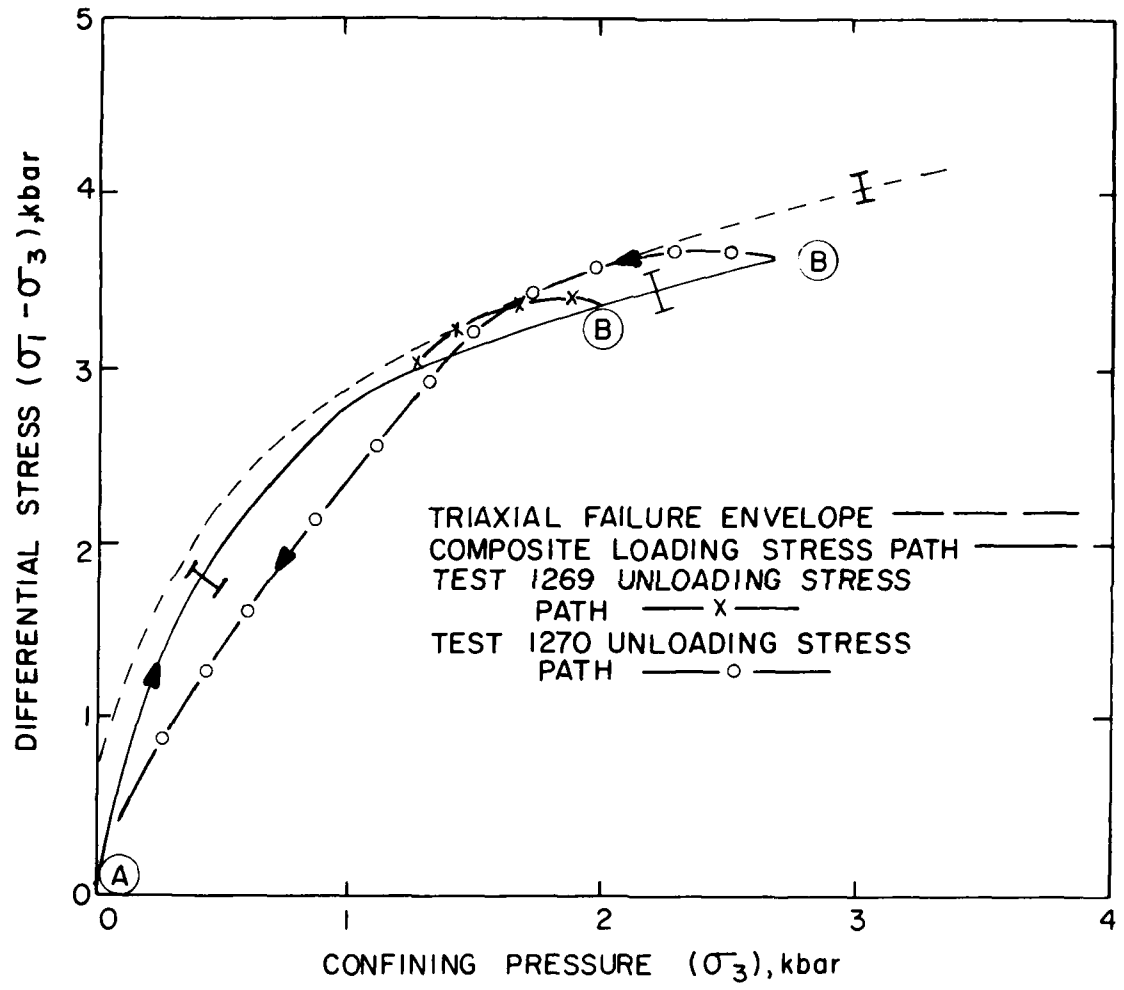


Figure 9a. Stress path followed during strain path III testing.

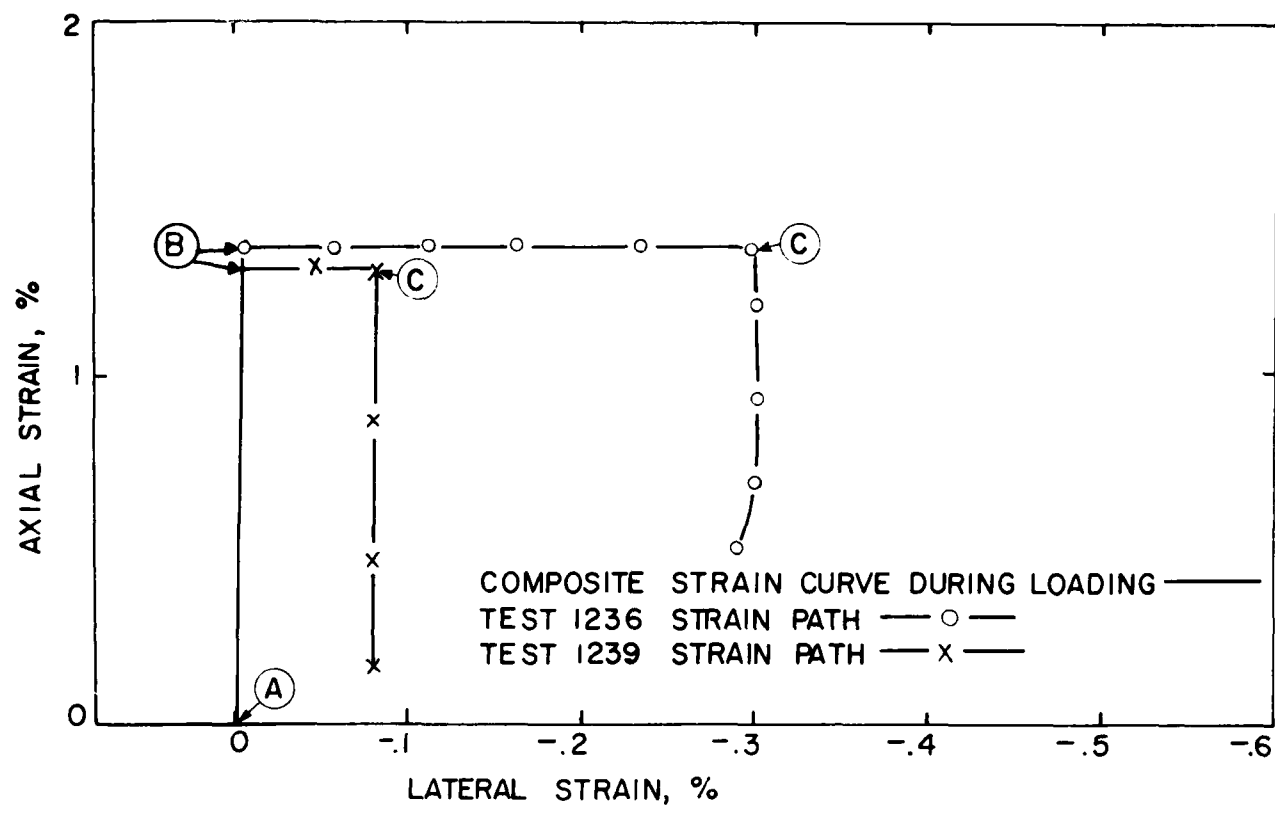


Figure 9b. Strain path followed during path I testing.

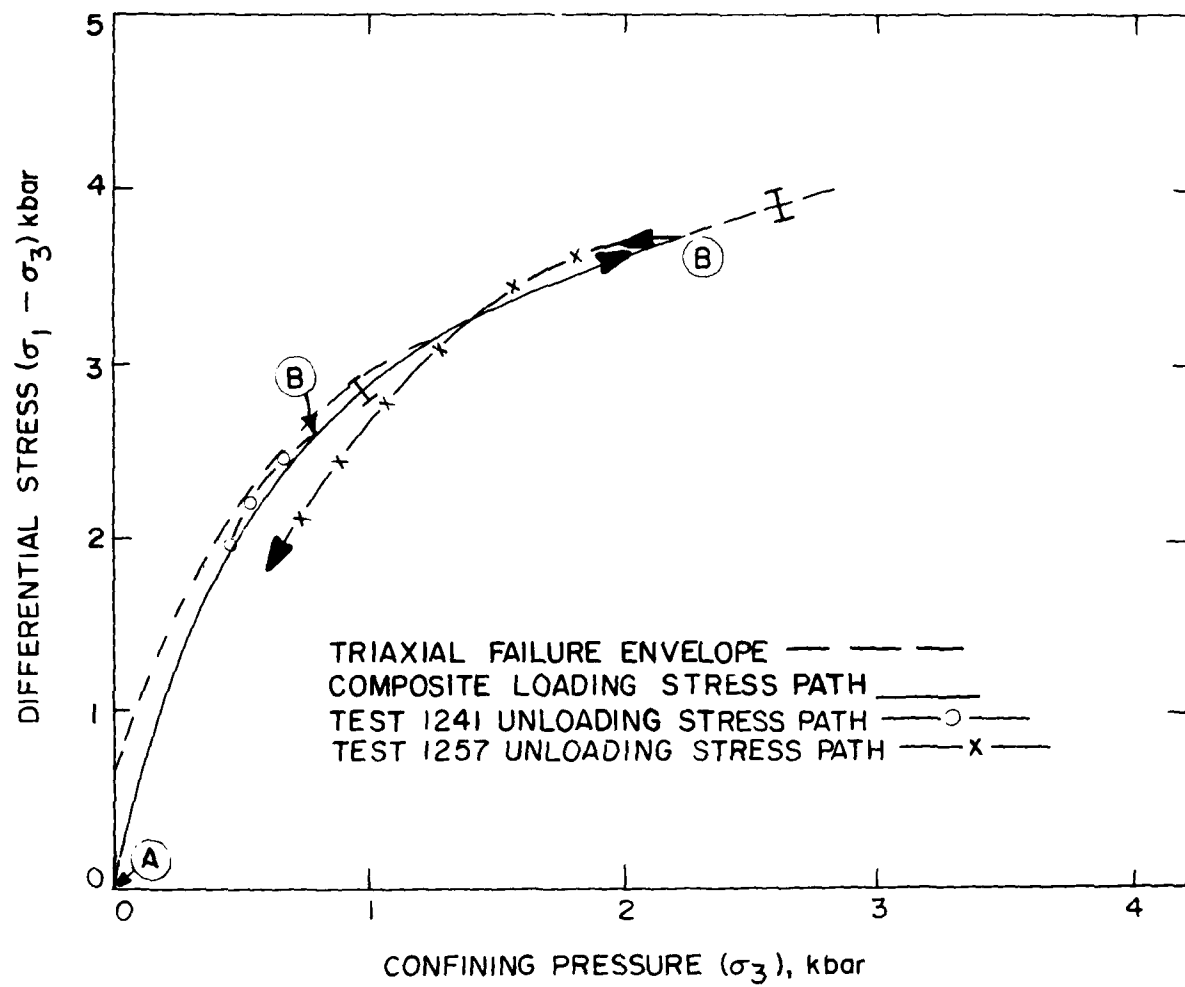


Figure 9c. Stress path followed during strain path II testing.

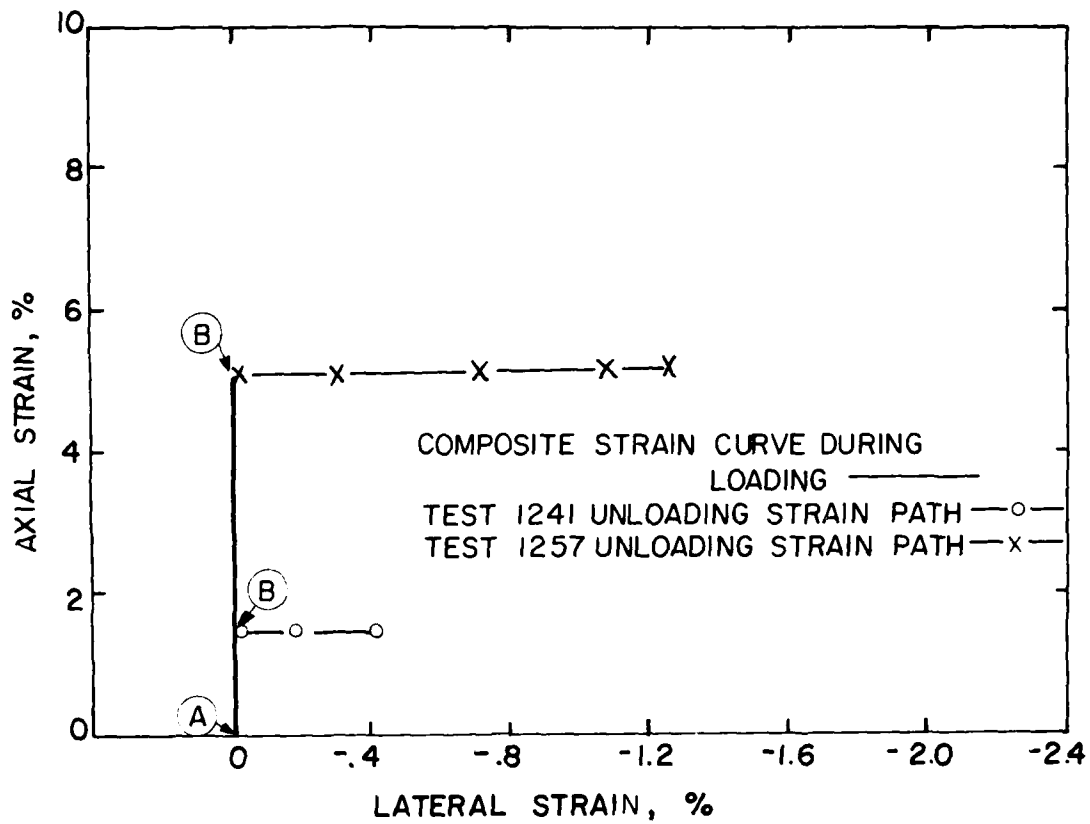


Figure 9d. Strain path followed during path II testing.

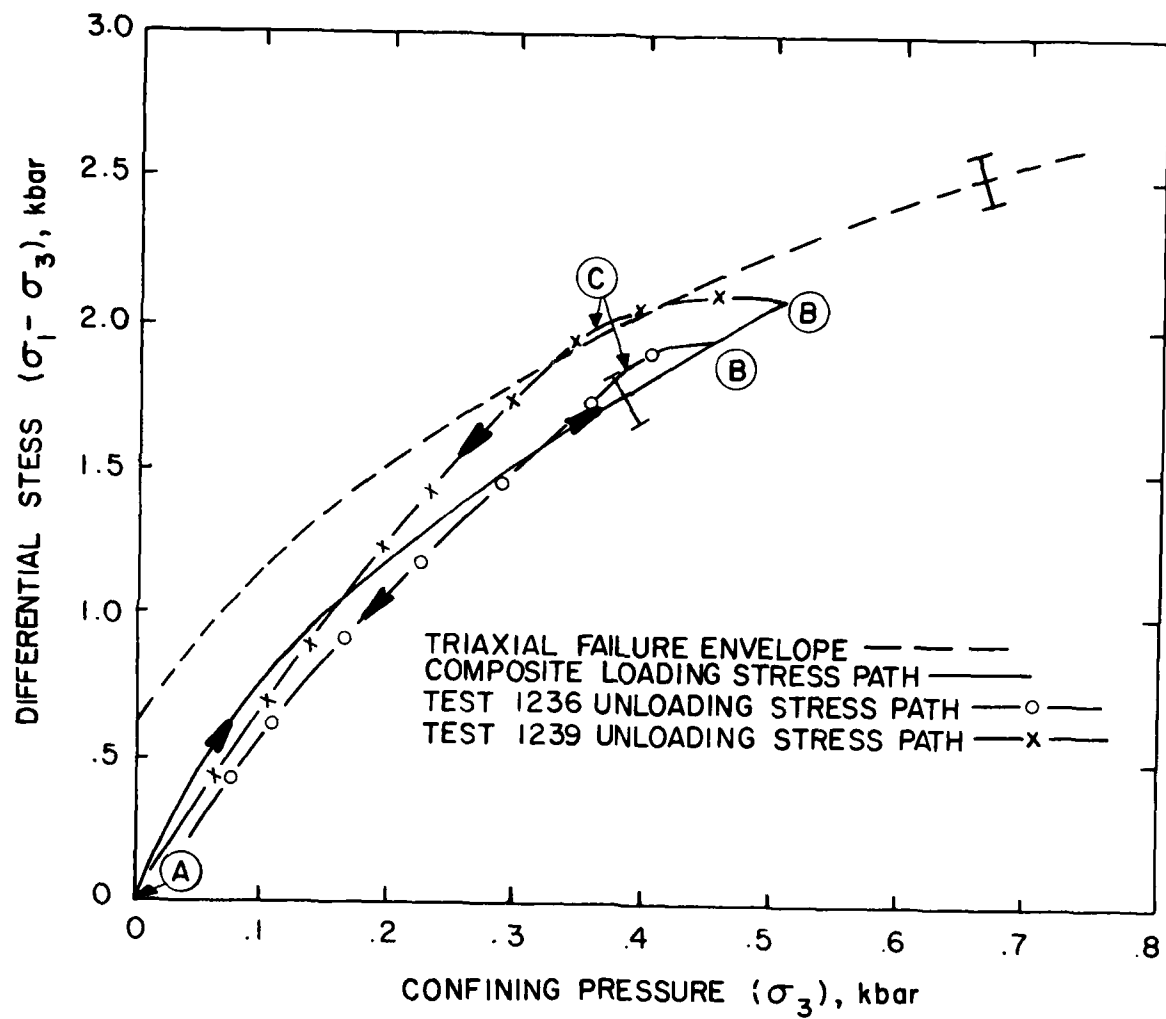


Figure 9e. Stress path followed during strain path I testing.

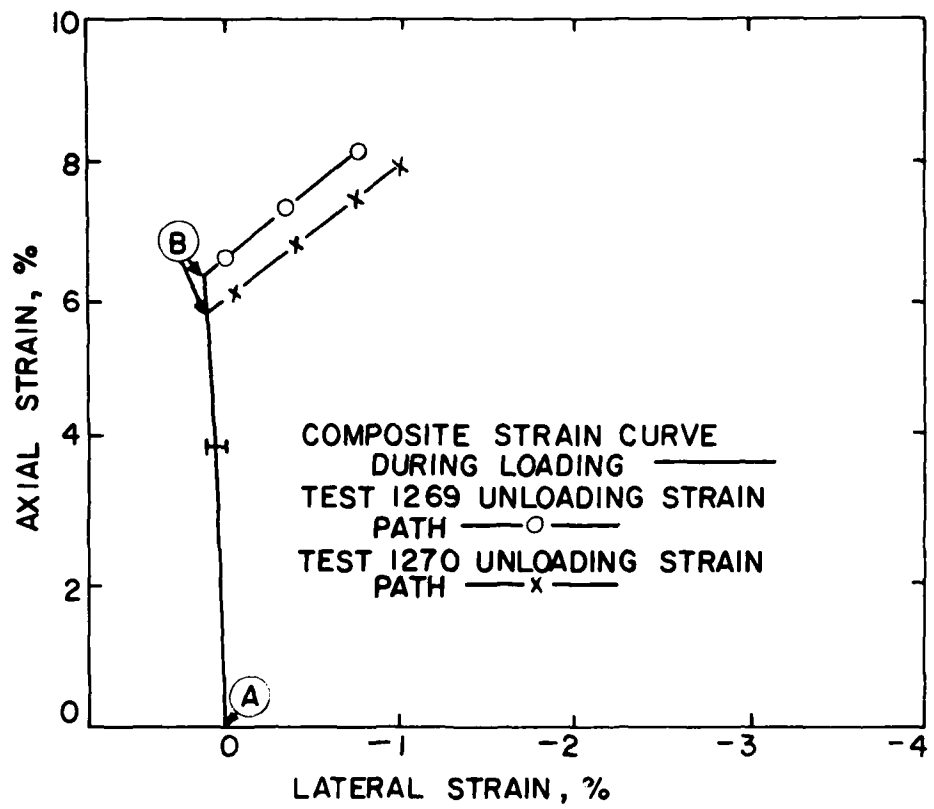


Figure 9f. Strain path followed during path III testing.

DISTRIBUTION LIST

DEPARTMENT OF DEFENSE

Assistant to the Secretary of Defense
 Atomic Energy
 ATTN: Executive Assistant

 Defense Advanced Rsch Proj Agency
 ATTN: G. Bulin

 Defense Intelligence Agency
 ATTN: DB-4N
 ATTN: DB-4C, E. O'Farrell

 Defense Nuclear Agency
 2 cy ATTN: SPSS
 4 cy ATTN: TITL

 Defense Technical Info Ctr
 12 cy ATTN: DD

 Field Command
 Defense Nuclear Agency
 ATTN: FCPR
 ATTN: FCTMOF

 Field Command
 Defense Nuclear Agency
 Livermore Branch
 ATTN: FCPRL

 Interservice Nuclear Weapons School
 ATTN: TTV

 Joint Strat Tot Planning Staff
 ATTN: JLA
 ATTN: NRI-STINFO Library

 NATO School (SHAPE)
 ATTN: U.S. Documents Officer

 Undersecretary of Defense for Rsch & Enrgy
 ATTN: Strategic & Space Systems (OS)

DEPARTMENT OF THE ARMY

BMD Advanced Technology Center
 Department of the Army
 ATTN: ATC-T
 ATTN: ICRDABH-X

 Chief of Engineers
 Department of the Army
 ATTN: DAEN-RDL
 ATTN: DAEN-MCE-D

 Harry Diamond Laboratories
 Department of the Army
 ATTN: DELHD-N-P
 ATTN: DELHD-I-TL

 U.S. Army Ballistic Research Labs
 ATTN: DRDAR-TSB-S
 ATTN: DRDAR-BLV
 ATTN: DADAR-BLT, J. Keefer

DEPARTMENT OF THE ARMY (Continued)

U.S. Army Concepts Analysis Agency
 ATTN: CSSA-ADL

 U.S. Army Engineer Center
 ATTN: DT-LRC

 U.S. Army Engineer Div Huntsville
 ATTN: HNDED-SR

 U.S. Army Engineer Div Ohio River
 ATTN: ORDAS-L

 U.S. Army Engr Waterways Exper Station
 ATTN: J. Drake
 ATTN: Library
 ATTN: WESSA, W. Flathau
 ATTN: WESSE, L. Ingram
 ATTN: J. Strange
 ATTN: J. Zelasko
 2 cy ATTN: VESSD, J. Jackson

 U.S. Army Materiel & Mechanics Rsch Ctr
 ATTN: Technical Library

 U.S. Army Materiel Dev & Readiness Cmd
 ATTN: DRXAM-TL

 U.S. Army Missile Command
 ATTN: RSIC

 U.S. Army Nuclear & Chemical Agency
 ATTN: Library

DEPARTMENT OF THE NAVY

Naval Civil Engineering Laboratory
 ATTN: Code L08A

 Naval Electronic Systems Command
 ATTN: PME 117-21

 Naval Facilities Engineering Cmd
 ATTN: Code 04B

 Naval Material Command
 ATTN: MAT 08T-22

 Naval Postgraduate School
 ATTN: G. Lindsay
 ATTN: Code 1424 Library

 Naval Research Laboratory
 ATTN: Code 2627

 Naval Surface Weapons Center
 ATTN: Code F31

 Naval Surface Weapons Center
 ATTN: Tech Library & Info Svcs Br

 Naval War College
 ATTN: Code E-11

DEPARTMENT OF THE NAVY (Continued)

Naval Weapons Evaluation Facility
ATTN: Code 10

Naval Underwater Systems Center
ATTN: Code EM, J. Kalinowski

Office of Naval Research
ATTN: Code 474, N. Perrone

Office of Chief of Naval Operations
ATTN: OP 981
ATTN: OP 03EG

Strategic Systems Project Office
Department of the Navy
ATTN: NSP-43

DEPARTMENT OF THE AIR FORCE

Air Force Geophysics Laboratory
ATTN: LWW, K. Thompson

Air Force Institute of Technology
ATTN: Library

Air Force Office of Scientific Rsch
ATTN: W. Best
ATTN: J. Allen

Air Force Systems Command
ATTN: DLW

Air Force Weapons Laboratory
Air Force Systems Command
ATTN: NTES-C, R. Henny
ATTN: NTES, J. Thomas
ATTN: NTE, M. Plamondon
ATTN: SUL
ATTN: NTES, R. Jolley

Air University Library
Department of the Air Force
ATTN: AUL-LSE

Assistant Chief of Staff
Intelligence
Department of the Air Force
ATTN: INT

Ballistic Missile Office
Air Force Systems Command
ATTN: MNN
ATTN: MNNXH, D. Game
ATTN: MNNXH, M. Delvecchio

Research, Development, & Acq
Department of the Air Force
ATTN: AFRD01

Logistics & Engineering
Department of the Air Force
ATTN: LEEE

Foreign Technology Division
Air Force Systems Command
ATTN: NTIS Library

DEPARTMENT OF THE AIR FORCE (Continued)

Rome Air Development Center
Air Force Systems Command
ATTN: TSLD

Strategic Air Command
Department of the Air Force
ATTN: INT J. McKinney
ATTN: NRI-STINFO Library

Vela Seismological Center
ATTN: G. Ullrich

DEPARTMENT OF ENERGY

Department of Energy
Albuquerque Operations Office
ATTN: CTID

Department of Energy
Nevada Operations Office
ATTN: Mail & Recds for Tech Lib

OTHER GOVERNMENT AGENCIES

Central Intelligence Agency
ATTN: OSWR/NED

Department of the Interior
Bureau of Mines
ATTN: Tech Lib

Federal Emergency Management Agency
ATTN: Assistant Associate Dir

DEPARTMENT OF ENERGY CONTRACTORS

Lawrence Livermore National Laboratory
ATTN: Tech Info Dept Lib
ATTN: D. Glenn

Los Alamos National Scientific Laboratory
ATTN: MS 670, J. Hopkins
ATTN: R. Bridwell
ATTN: MS 364

Oak Ridge National Laboratory
Nuclear Division
ATTN: Central Rsch Lib
ATTN: Civil Def Res Proj

Sandia National Laboratories
Livermore Laboratory
ATTN: Lib & Sec Class Div

Sandia National Laboratories
ATTN: L. Hill
ATTN: A. Chabai
ATTN: 3141

DEPARTMENT OF DEFENSE CONTRACTORS

Aerospace Corp
ATTN: Technical Info Svcs

Ababian Associates
ATTN: M. Ababian

DEPARTMENT OF DEFENSE CONTRACTORS (Continued)

Applied Research Associates, Inc.

ATTN: H. Auld
ATTN: N. Higgins
ATTN: J. Bratton

Applied Research Associates, Inc

ATTN: S. Blouin

Applied Theory, Inc

2 cy ATTN: J. Trulio

AVCO Research & Systems Group

ATTN: Library A830

BDM Corp

ATTN: Corporate Library
ATTN: T. Neighbors

Boeing Co

ATTN: Aerospace Library

California Institute of Technology

ATTN: T. Ahrens

California Research & Technology, Inc

ATTN: K. Kreyenhagen
ATTN: Library
ATTN: M. Rosenblatt
ATTN: S. Schuster

California Research & Technology, Inc

ATTN: D. Orphal

Calspan Corp

ATTN: Library

University of Denver

ATTN: J. Wisotski

EG&G Washington Analytical Svcs Ctr, Inc

ATTN: Library

Eric H. Wang

Civil Engineering Rsch Fac
University of New Mexico
ATTN: N. Baum

Gard, Inc

ATTN: G. Neidhardt

Horizons Technology, Inc

ATTN: R. Kruger

IIT Research Institute

ATTN: Documents Library
ATTN: R. Welch
ATTN: M. Johnson

Institute for Defense Analyses

ATTN: Classified Library

J.H. Wiggins Co., Inc

ATTN: J. Collins

DEPARTMENT OF DEFENSE CONTRACTORS (Continued)

Kaman AviDyne

ATTN: N. Hobbs

ATTN: Library

Kaman Sciences Corp

ATTN: Library

Kaman Tempo

ATTN: DASIAC

Lockheed Missiles & Space Co., Inc

ATTN: T. Geers

ATTN: Technical Info Ctr

Lockheed Missiles & Space Co., Inc

ATTN: J. Weisner

Lovelace Biomed & Enviro Rch Inst, Inc

ATTN: R. Jones

Martin Marietta Corp

ATTN: G. Freyer

McDonnell Douglas Corp

ATTN: R. Halprin

Merritt CASES, Inc

ATTN: J. Merritt

ATTN: Library

Pacific-Sierra Research Corp

ATTN: H. Brode

Patel Enterprises, Inc

ATTN: M. Patel

Physics International Co

ATTN: L. Behrmann

ATTN: F. Sauer

ATTN: E. Moore

ATTN: Technical Library

ATTN: J. Thomsen

R & D Associates

ATTN: Technical Info Ctr

ATTN: J. Lewis

ATTN: J. Carpenter

ATTN: W. Wright

ATTN: R. Port

ATTN: P. Haas

Science Applications, Inc

ATTN: Technical Library

Science Applications, Inc

ATTN: D. Bernstein

ATTN: D. Maxwell

Science Applications, Inc

ATTN: W. Layson

Southwest Research Institute

ATTN: W. Baker

ATTN: A. Wenzel

DEPARTMENT OF DEFENSE CONTRACTORS (Continued)

SRI International

ATTN: D. Keough
ATTN: G. Abrahamson
ATTN: B. Gasten
ATTN: Y. Gupta

Systems, Science & Software, Inc

ATTN: T. Cherry
ATTN: T. Riney
ATTN: Library
ATTN: D. Grine

Systems, Science & Software, Inc

ATTN: J. Murphy

Terra Tek, Inc

ATTN: S. Green
ATTN: A. Abou-Sayed
ATTN: Library
4 cy ATTN: J. Johnson
4 cy ATTN: D. Schmitz
4 cy ATTN: R. Dronek

DEPARTMENT OF DEFENSE CONTRACTORS (Continued)

Tetra Tech, Inc

ATTN: L. Hwang

TRW Defense & Space Sys Group

ATTN: Technical Info Ctr
ATTN: P. Bhutta
2 cy ATTN: N. Lipner

TRW Defense & Space Sys Group

ATTN: P. Dai
ATTN: E. Wong

Universal Analytics, Inc

ATTN: E. Field

Weidlinger Assoc., Consulting Engineers

ATTN: M. Baron

Weidlinger Assoc., Consulting Engineers

ATTN: J. Isenberg

